THE JOURNAL OF BIOLOGICAL CHEMISTRY VOL. 287, NO. 49, pp. 41481–41498, November 30, 2012
Published in the U.S.A.

HIV-1 Nef Impairs Heterotrimeric G-protein Signaling by Targeting $G\alpha_{i2}$ for Degradation through Ubiquitination*

Received for publication, March 16, 2012, and in revised form, October 12, 2012 Published, JBC Papers in Press, October 15, 2012, DOI 10.1074/jbc.M112.361782

Prabha Chandrasekaran[‡], Monica Buckley[‡], Victoria Moore[‡], Long Qin Wang[‡], John H. Kehrl[§], and Sundararajan Venkatesan[‡1]

From the [‡]Laboratory of Molecular Immunology and [§]Laboratory of Immunoregulation, NIAID, National Institutes of Health, Bethesda, Maryland 20892

Background: HIV Nef disrupts chemotaxis of immune cells by targeting multiple steps.
Results: Nef recruits AIP4 E3 ligase, to ubiquitinate $G\alpha_{i2}$ of heterotrimeric G-proteins for subsequent lysosomal degradation.
Conclusion: Nef impedes chemokine-signaling events via degradation of $G\alpha_{i2}$.
Significance: Impaired G-protein signaling by HIV Nef-expressing lymphocytes probably contributes to immune dysfunction in AIDS.

The HIV Nef protein is an important pathogenic factor that modulates cell surface receptor trafficking and impairs cell motility, presumably by interfering at multiple steps with chemotactic receptor signaling. Here, we report that a dominant effect of Nef is to trigger AIP4 E3 ligase-mediated $G\alpha_{i2}$ ubiquitination, which leads to $G\alpha_{i2}$ endolysosomal sequestration and destruction. The loss of the $G\alpha_{i2}$ subunit was demonstrable in many cell types in the context of gene transfection, HIV infection, or Nef protein transduction. Nef directly interacts with $G\alpha_{i2}$ and ternary complexes containing AIP4, Nef, and $G\alpha_{i2}$ form. A substantial reversal of $G\alpha_{i2}$ loss and a partial recovery of impaired chemotaxis occurred following siRNA knockdown of AIP4 or NEDD4 or by inhibiting dynamin. The N-terminal myristoyl group, ^{62}EEEE^{65} motif, and ^{72}P*XX*P^{75} motif of Nef are critical for this effect to occur. Nef expression does not affect a Gq_{i5} chimera where the five C-terminal residues of Gq are replaced with those of $G\alpha_{i2}$. Lysine at position 296 of $G\alpha_{i2}$ was identified as the critical determinant of Nef-induced degradation. By specifically degrading $G\alpha_{i2}$, Nef directly subverts leukocyte migration and homing. Impaired trafficking and homing of HIV Nef-expressing lymphocytes probably contributes to early immune dysfunction following HIV infection.

The recirculation of naive and memory lymphocytes, the trafficking of lymphocytes into lymphoid organs, and the appropriate localization of effector cells depend upon a regulated configuration of cell surface adhesion molecules and chemoattractants. Ligand-occupied chemoattractant receptors, trigger $G\alpha$ subunits of the heterotrimeric G-protein G_i to exchange GTP for GDP. This leads to the release of $G\alpha_i$-associated $G\beta\gamma$ subunits, activation of downstream effectors, and directed cell migration (1). T lymphocytes employ several different chemokine receptors. The chemokine receptors CCR7, CCR9, and CXCR4 (chemokine (C*X*C motif) receptor 4) along with their cognate ligands regulate T-cell ontogeny in the thymus (2–4), whereas CCR7 regulates the migration of peripheral T cells to lymphoid tissue during adaptive immune response (5, 6). Proinflammatory chemokine receptors like CXCR3 and CCR5 and their respective ligands regulate effector CD4 and CD8 T cell trafficking in peripheral tissues (7–10). During an adaptive immune response, activated paracortical T cells use CCR7 and CXCR5 to migrate to the follicle edge and eventually into the lymph node follicle, where they help coordinate B lymphocyte responses (11, 12). Impaired signaling through these different receptors can cause immune dysfunction and lymphoid tissue disorganization.

A hallmark of HIV infection is severe disruption of the cellular microenvironment of lymph nodes and the gastrointestinal associated lymphoid tissue. Although this occurs in part as a consequence of $CD4^+$ T cell depletion, a major contributing factor is compromised chemoattractant receptor signaling (13, 14). Perinatal HIV infection results in profound T cell developmental abnormalities mimicking those observed in thymic dysplasia in DiGeorge syndrome (15). Implicating the HIV Nef protein as a major co-factor in the general pathology and immune dysfunction in HIV AIDS, transgenic mice expressing HIV-1 provirus or HIV Nef protein alone have a similar constellation of immune pathologies (16–18).

Several mechanisms have been found by which Nef can interfere with chemoattractant receptor signaling. First, HIV and SIV Nef proteins have been shown to down-regulate chemokine receptor expression, presumably through enhanced receptor endocytosis (19, 20). This has been associated with a marked chemotactic arrest, presumably due to loss of the cognate receptor (19). Second, Nef can interfere with signal transduction pathways downstream of the receptors by affecting different intracellular signaling proteins involved in these pathways. These include the Ser/Thr kinase PAK; small GTPases, such as Rac and CDC42; and guanine nucleotide exchange factors, such as Vav and DOCK2-ELMO1 (21–24). In particular, Nef inhibited T lymphocyte chemotaxis toward CXCL12 (chemokine (C*X*C motif) ligand 12) by disrupting spatially organized cytoskeleton rearrangements through unregulated DOCK2-ELMO1-mediated Rac activation (24). Third, Nef has been

* This work was supported, in whole or in part, by the National Institutes of Health, NIAID, Intramural Research Program.
[1] To whom correspondence should be addressed: LMI, NIAID, Bldg. 10, Rm. 11N117, National Institutes of Health, Bethesda, MD 20892. Tel.: 301-404-1054; E-mail: sv1s@nih.gov.

linked to decreases in integrin expression, which impaired transmigration across endothelial cells (25). Fourth, Nef expression can alter the morphology of T lymphocytes and dendritic cells through changes in F-actin dynamics (26–28) by deregulating cofilin through PAK2 interaction (29) and RhoA interaction with diaphanous interacting protein and p190RhoAGAP (30). With the exception of the studies implicating reduced receptor expression, the majority of these studies indicate that the prominent effect of Nef on chemokine and chemoattractant receptor signaling is downstream of the major signal transducer, the heterotrimeric G-protein G_i.

Although Nef undoubtedly targets multiple sites in the chemoattractant signaling pathway, we have discovered a dominant effect of Nef because its expression results in a marked loss of steady-state levels of $G\alpha_{i2}$ protein but not of other $G\alpha$ or $G\beta\gamma$ subunits. Nef triggered AIP4 (atrophin-interacting protein 4) E3 ligase-mediated $G\alpha_{i2}$ ubiquitination, leading to its endolysosomal sequestration and destruction. The consequence of the loss of $G\alpha_{i2}$ is a marked impairment in chemoattractant receptor signaling and directed leukocyte migration.

EXPERIMENTAL PROCEDURES

Expression Plasmids—Expression plasmids for CD4, CD8, WT and mutant Nef alleles, Nef Cerulean, and bicistronic IRES[2] plasmids encoding Nef and GFP have been described (31). Chemokine receptors, YFP-tagged $G\alpha_i$ subunits, and the Gq_{i5} chimera have been described (32–36). Mutations replacing each one of the three lysines at positions 296, 307, and 314 of $G\alpha_{i2}$ (but not in $G\alpha_{i3}$) with arginines were engineered by PCR mutagenesis of YFP-tagged $G\alpha_{i2}$ (35). The GST-Nef construct was constructed by in-frame cloning of Nef ORF into the EcoRI-SalI sites of pGEX-4T1 (GE Healthcare). Plasmids expressing GST fused to full-length AIP4, AIP4ΔWW, and AIP4-WW-I-IV were generously supplied by Adriano Marchese (Stritch School of Medicine, Loyola University, Chicago) as were the expression plasmids for FLAG-ubiquitin, FLAG-tagged WT AIP4, or c-Myc-tagged WT or C830A AIP4 mutant. The GST fusion proteins were expressed in *Escherichia coli* strain XL-1 Blue (Stratagene) and purified according to the manufacturer's (GE Healthcare) instructions.

Antibodies and Reagents—The following reagents were obtained from commercial sources. Unconjugated or dye-conjugated mAbs against EEA1 (early endosomal antigen 1) actin were from BD Immunocytometry (San Diego, CA); unconjugated LAMP1 (H4A3) and LAMP2 (H4B4) mAbs were from the Developmental Studies Hybridoma Bank (University of Iowa, Iowa City, IA); unconjugated or Alexa 488-, 647-, allophycocyanin-, or phycoerythrin-conjugated CD4 and CD8 were from Invitrogen or R&D Systems; antibodies against AIP4 and NEDD4, murine anti-$G\alpha_{i2}$ mAb, rabbit polyclonal antibodies against $G\alpha_{i2}$ (sc-7276), $G\alpha_{i3}$ (sc-262), $G\alpha_o$ (sc-387), $G\alpha_{q/11}$ (sc-392), and $G\alpha_{13}$ (sc-410), and goat polyclonal antibody against actin (sc-1615) were from Santa Cruz Biotechnology, Inc. (Santa Cruz, CA); anti-YFP mAb was from Clontech Corp.; and rabbit IgG and murine mAb against HA or FLAG epitopes were from Covance or Roche Applied Science and Sigma-Aldrich, respectively. A second rabbit polyclonal antibody against $G\alpha_o$ (catalog number 3975) was purchased from Cell Signaling Technology (Danvers, MA). Secondary antibodies to mouse, rabbit, goat, and human IgG conjugated to various Alexa dyes were from Invitrogen Corp., and HRP-conjugated goat anti-mouse, rabbit, or human IgG and donkey anti-goat IgG were from Pierce. Dyansore was purchased from Tocris Corp.; epoxomicin, forskolin, isoproterenol, and MG-132 were from EMD Biosciences. Dynasore and epoxomicin treatments were used at 80 and 25 μM concentrations, respectively, for 4 h at 37 °C, followed by staining for flow cytometry or immunoblotting.

Cells and Transfection—For this study, HeLa cells were used for microscopy, and T cell lines of Jurkat or CEM cells were used for phenotypic assays. HeLa cell transfection conditions have been described in detail before (69). The Department of Transfusion Medicine at the National Institutes of Health provided elutriated monocytes and leukocyte-enriched buffy coat from anonymous volunteers. Peripheral blood lymphocytes were purified as before (69), and cells were cultivated under standard conditions in RPMI medium or DMEM with 10% fetal calf serum (FCS) and 1% L-glutamine, as appropriate. Primary hematopoietic cells and cell lines in suspension ($7–10 \times 10^6$ cells/100 μl) were nucleofected with 3–5 μg of DNA using an Amaxa Nucleofector as recommended by the manufacturer. In all cases, GFP or CD8 expression plasmid was included to check transfection efficiency as described (31). Cell viability was checked using a FACS-based live/killed assay kit using a Guava Easycyte flow cytometer as described by the manufacturer (Millipore Corp.). Experiments were rejected if cell viability was less than 75%. For biochemical experiments, cell numbers were adjusted to equivalent viability and transfection efficiency. However, for most non-FACS-based experiments, transfectants were purified by positive selection using CD8 immunoaffinity beads from Stem Cell Technologies as recommended by the manufacturer.

HIV Infection—For single-cycle HIV infection, recombinant viruses expressing mouse CD24 in place of vpR (CD24), CD24 with a vpU deletion (CD24U), or CD24 lacking both vpU and Nef (CD24UM1T) were generated by 293-T cell transfection (Trans-IT LT1 transfection reagent, Mirus Corp.) with the respective HIV proviruses and a VSV-G expression plasmid. Infection was allowed to proceed for 48–72 h to achieve >40% infection. Virus production, quantification, and T cell infection kinetics have been described before (33).

RNA-mediated Interference—$G\alpha_{i1}$, $G\alpha_{i2}$, $G\alpha_{i3}$, and $G\alpha_o$ subunits were knocked down using the recommended sequence (37). AIP4 and NEDD4 were knocked down using UUUCAAUGCAGAAUUUCUGUGGUCC and UAGAGGAGAAGGUUCUUGUUGUUGC, respectively (Invitrogen). Protocols for siRNA transfection followed by plasmid expression have been described before (31).

Intracellular [Ca^{2+}] Measurements—Two different spectrofluorimetric assays were used. In the ratiometric assay, the rel-

[2] The abbreviations used are: IRES, internal ribosome entry site; CerFP, Cerulean fluorescent protein; HECT, homologous to E6-AP C terminus; CFP, cyan fluorescent protein; ER, endoplasmic reticulum; ESCRT, endosomal sorting complex required for transport; GPCR, G-protein-coupled receptor; LAMP, lysosome-associated membrane protein; PBMC, peripheral blood mononuclear cell; PM, plasma membrane; ROI, region of interest; VSV, vesicular stomatitis virus.

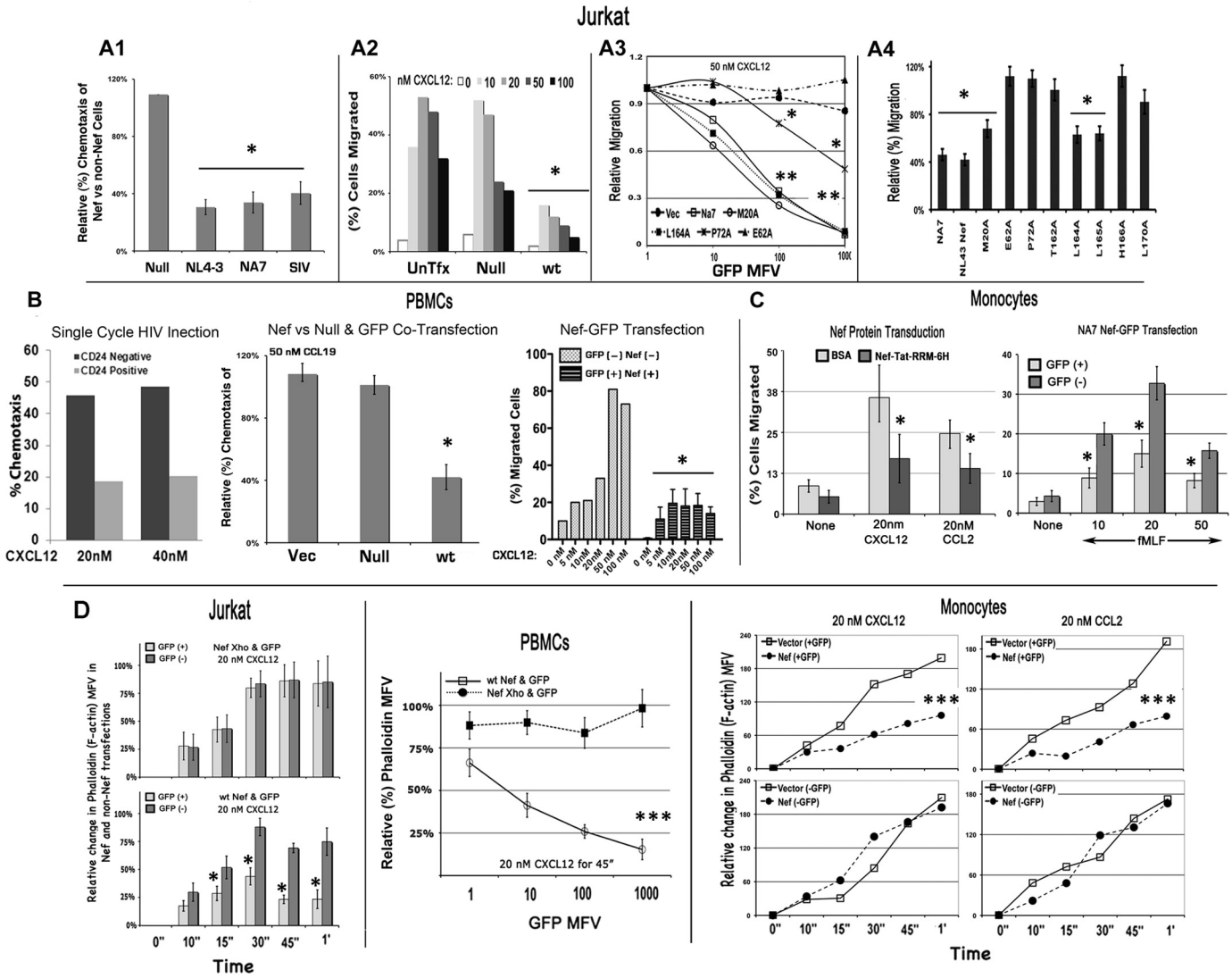

FIGURE 1. **Nef inhibits migration of Jurkat T cells (*A1–A4*), fresh PBMCs (*B*), and monocytes (*C*) toward CXCL12 in a transwell assay and F-actin accumulation in response to CXCL12 or CCL2 (*D*).** Relative (%) chemotaxis of Jurkat cells expressing different Nef alleles (and gated for GFP co-expression) at the optimal peak levels of CXCL12 for cells is illustrated by the histogram (mean with S.E., $n = 3$; *, $p < 0.01$) in *A1*, and a representative CXCL12 dose-response profile of chemotaxis of Nef(−) or Nef(+) cells ($n = 3$) is illustrated in *A2*. Relative migration potential of Jurkat cells expressing GFP alone (*Vec*) or with WT NA7, M20A, P72A, E62A, or L164A mutant from Nef-GFP IRES vector toward CXCR4 is shown as a function of GFP expression in *A3* ($n = 3$). *, $p < 0.05$; **, $p < 0.01$, when compared with plasmid-transfected cells. *A4*, relative (%) chemotaxis of Jurkat cells transfected with CD8 alone or with WT NA7 or NL4–3 Nef allele or M20A, P72A, E62A, or L164A NL4–3 Nef mutant. Chemotaxis data are shown for CD8(+) cells ($n = 3$). *, $p < 0.01$ compared with respect to null controls. *B*, the histogram on the *left* shows chemotaxis potential of single-cycle Nef(+) HIV-infected (CD24-positive) and uninfected (CD24-negative) CEM cells toward CXCL12. Relative (%) migration potential of CEM cells in WT infected ($CD24^+$) and non-infected ($CD24^-$) population to different concentrations of CXCL12 was assessed by a transwell migration assay. The next histogram (with *error bars* (S.E.)) shows relative (%) chemotaxis toward CCL19 of PBMCs cotransfected with GFP and WT Nef, null mutant, or empty vector ($n = 3$, $p < 0.02$). CXCL12 dose response of chemotaxis (in absolute terms) for Nef(+) GFP(+) *versus* Nef(−) GFP(+) transfectants is illustrated on the *right* ($n = 3$). *, $p < 0.05$ compared with respective nanomolar concentration. *C*, histograms with S.E. ($n = 3$) show the chemotaxis potential toward CXCL12 or CCL2 (*left*) and formylmethionylleucylphenylalanine (*right*) of monocytes, transduced for 2 h with BSA or purified Nef fusion protein tagged C-terminally with the arginine-rich motif (*RRM*) of HIV-1 Tat followed by His_6 residues ($n = 3$). *, $p < 0.05$. *D*, time course of F-actin accumulation in Jurkat cells or fresh PBMCs nucleofected with bicistronic (IRES) plasmids encoding WT or null (Nef Xho) Nef and GFP. Histograms (with S.E.) on the *left* illustrate the F-actin accumulation in GFP(+) *versus* GFP(−) gated Jurkat cells nucleofected with Nef-Xho-IRES-GFP (*top*) or Nef-IRES-GFP (*bottom*) ($n = 3$). *, $p < 0.02$. PBMCs nucleofected with Nef-IRES-GFP or NefXho-IRES-GFP were treated with 20 nM CXCL12 for 45 min. Relative (%) F-actin levels (phalloidin mean fluorescence value (*MFV*)) are plotted as a function of GFP (Nef or NefXho) expression ($n = 3$). *Bars*, S.E.; ***, $p < 0.01$. Alternatively, monocytes were nucleofected with GFP and Nef or an empty vector, and the time course of F-actin accumulation in response to 20 nM CXCL12 or CCL2 was monitored in GFP(−) *versus* GFP(+) cells ($n = 3$). ***, $p < 0.05$.

ative ratio of fluorescence emitted at 510 nm after sequential excitation at 340 and 380 nm was measured as described (33), using Fura-2 AM (Invitrogen) as the calcium-binding dye in a fluorimeter (Photon Technology Inc., South Brunswick, NJ). Alternatively, intracellular Ca^{2+} levels were measured using a FLIPR 3 calcium assay kit (Molecular Devices) with a FlexStation III scanning fluorimeter as described (38), using Softmax Pro (Molecular Devices) for data acquisition and analysis. Single cell analysis of calcium flux was performed using the Leica SP5, using a ×40 oil immersion objective, numerical aperture 1.25. HeLa cells in 8-well chambers (LabTek chambers, Thermo Scientific) were cotransfected with CerFP or Nef-CerFP and YFP-tagged WT Gα$_{i2}$ or Gα$_{i3}$. At 18–24 h post-transfection, cells were loaded with Hanks' balanced

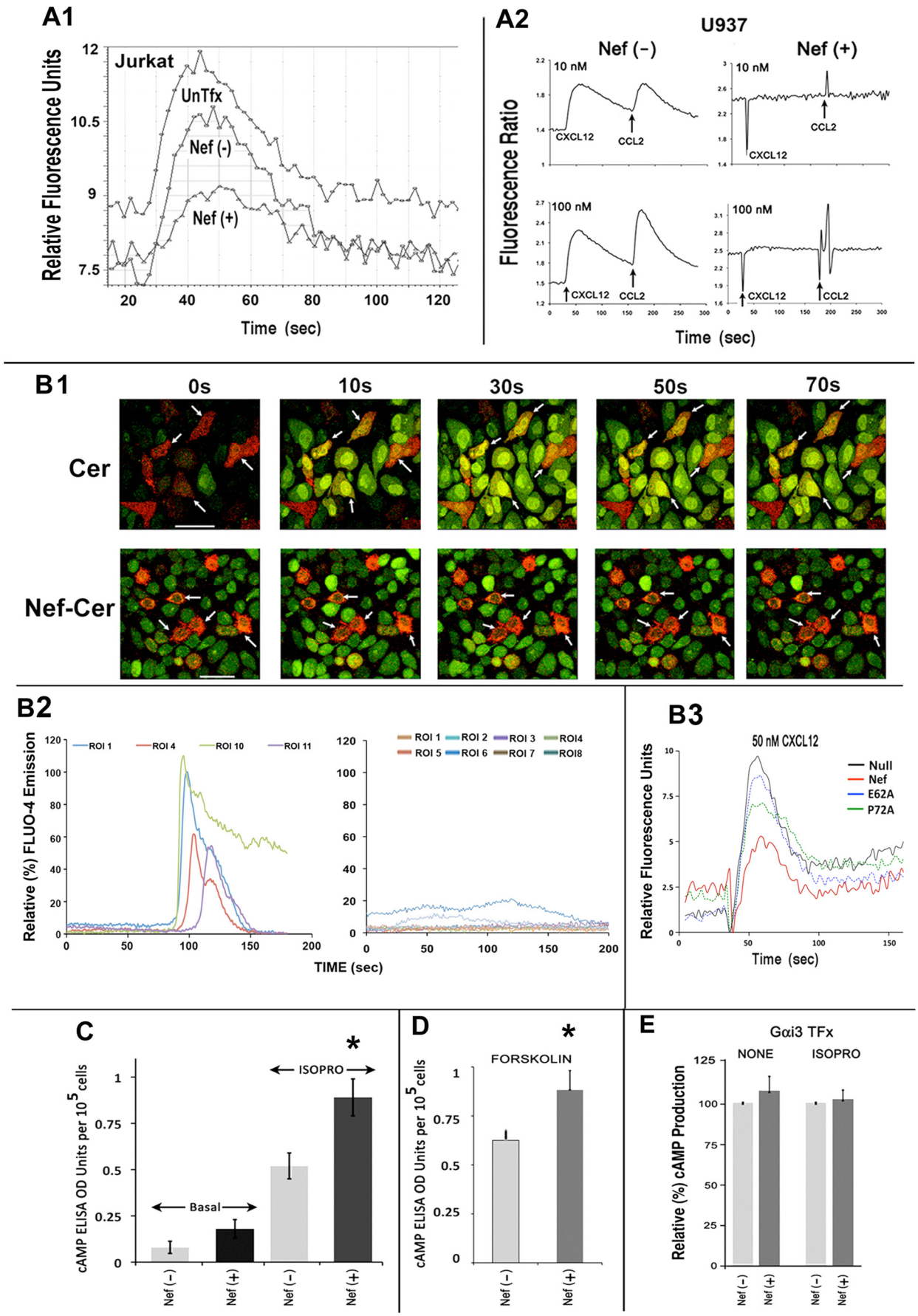
A1
Jurkat
UnTfx
Nef (-)
Nef (+)
Relative Fluorescence Units
Time (sec)
A2
U937
Nef (-)
Nef (+)
10 nM
100 nM
CXCL12
CCL2
Fluorescence Ratio
Time (sec)
B1
0s
10s
30s
50s
70s
Cer
Nef-Cer
B2
ROI 1
ROI 4
ROI 10
ROI 11
ROI 2
ROI 3
ROI4
ROI 5
ROI 6
ROI 7
ROI8
Relative (%) FLUO-4 Emission
TIME (sec)
B3
50 nM CXCL12
Null
Nef
E62A
P72A
Relative Fluorescence Units
Time (sec)
C
ISOPRO
Basal
cAMP ELISA OD Units per 10^5 cells
Nef (-)
Nef (+)
D
FORSKOLIN
cAMP ELISA OD Units per 10^5 cells
E
Gαi3 TFx
NONE
ISOPRO
Relative (%) cAMP Production

saline solution containing Ca^{2+} and Mg^{2+} (Invitrogen) with 1% FBS and 4 μM Fluo-4 AM (Invitrogen). The cells were irradiated with a UV laser at 405 nm for Cerulean and with an argon laser at 488 nm for Fluo-4 and at 514 nm for YFP. Images were acquired in a 512 × 400-pixel format with the pinhole set at 2 airy units every 1–1.4 s for ~200 s. The images were collected as line scan images, which provide the values of the calcium-dependent increase in fluorescence along a single spatial dimension as a function of time. For analysis, the regions of interest (ROIs) were drawn on the cells expressing Cerulean/Nef Cerulean. At least 10 ROIs were drawn for each field, and the calcium flux was measured in >5 fields for each experimental condition. The change in the intensities was analyzed using the Leica software, followed by graphing using EXCEL.

Affinity Selections—GST pull-downs of cellular extracts (10^7 cell equivalents in 1 ml) in 25 mM Tris-HCl, pH 7.4, 150 mM NaCl, 1 mM EGTA, 0.5 mM $MgCl_2$, and 0.5% (w/v) Triton X-100 (lysis buffer) with protease inhibitors (1 Complete tablet/ml; Roche Applied Science) was done using purified GST or the indicated GST fusion proteins immobilized on glutathione- agarose beads (GE Healthcare) and incubated for 2 h. The beads were washed three times with lysis buffer and once with lysis buffer without Triton X-100. Bound proteins were resolved by SDS-PAGE and detected by immunoblotting using antibodies against the respective targets. His_6-tagged Nef protein was affinity-selected from extracts of corresponding transfectants using Ni^{2+}-nitrilotriacetic acid-agarose beads (Qiagen Corp.), and FLAG-tagged proteins were selected using agarose bead immobilized M2 mAb (Sigma-Aldrich).

cAMP Assay—Intracellular cAMP levels were assayed using the Direct cAMP Enzyme Immunoassay kit (Assay Designs), following the manufacturer's instructions. The optical density was read at 405 nm in a FlexStation II microplate scanner, and the results were analyzed using Softmax Pro 5 (Molecular Devices, Sunnyvale, CA).

Flow Cytometry—The fluorescent dye-conjugated antibodies for CD4, CD8, and the chemokine receptors were obtained from BD Biosciences, R&D Systems, or eBioscience. One million cells were incubated with the appropriate antibodies in 100 μl of PBS containing 1% goat serum for 15 min at room temperature. The data acquisition was carried out using a FACSort™ (BD Biosciences) flow cytometer, and the analyses were done using FlowJo version 9.2. (Tree Star Inc., Ashland, OR). Flow cytometric detection of F-actin by phalloidin staining has been described (75).

Confocal Microscopy—Confocal microscopy was done as described (32) using a Leica TCS-NT/SP5 microscope (Leica, Exton, PA) equipped with a 100× oil immersion objective, numerical aperture 1.32. Images were collected using digital zooms up to ×8. Co-localization experiments were done with live (fluorescent proteins) or fixed cells for most experiments as described (31). The fluorochromes were excited using a UV laser at 405 nm for Cerulean, an argon laser at 488 nm for Alexa 488 and YFP, and a DPSS laser at 561 nm for Alexa 568 and 647. Images were processed using the Leica TCS-NT/SP5 software, Leica Lite, and Adobe Photoshop CS4.

FRET Assay—FRET interactions between Nef-CerFP and YFP-tagged $G\alpha_{i2}$ or $G\alpha_{i3}$ were evaluated using the Leica acceptor photobleaching software to examine in live or fixed cells in the Leica SP5 confocal microscope with a ×60, numerical aperture 1.4 oil immersion objective in a 512 × 512-pixel format using a DPSS laser at 442 nm for Cerulean and an argon laser at 514 nm for YFP. The exposure times were kept equal within each series of images and chosen such that all pixel intensities were within the linear range. A ×63 oil lens was used unless mentioned otherwise. ROIs were selected from individual fields visualized at zoom factors between 1 and 8 (Z1–Z8), and 50–80% YFP photobleaching was achieved in the selected ROIs using the 514-nm laser at 100% power for 45 s at ×8 optical zoom. Each pixel of the image contains data corresponding to an emission spectrum resulting from both CFP and YFP. The fluorescence intensities of donor and acceptor were measured before and after photobleaching in the ROIs drawn at different cellular organelles and membranes. The diameter of the ROIs was kept uniform throughout the analysis at 8 μm. 10 ROIs were drawn for each part of a single cell, and at least 10 different cells were taken for each FRET efficiency calculation. Only regions photobleached at >50% were considered for analysis. FRET efficiency was calculated using the equation $E_F = (I_{\text{postbleach}} - I_{\text{prebleach}})/I_{\text{postbleach}}$, where I is the average CFP fluorescence intensity after the subtraction of the background.

Chemotaxis Assays—End-point chemotaxis was determined using the transwell system with membranes of 6.5-mm diameter and 5.0-μm pore size in RPMI containing 10 mM HEPES and 1% FBS as described (32). The ratios of migrated cells were determined from the number of cells in the lower and upper

FIGURE 2. **Nef markedly inhibited biochemical readouts of $G\alpha_{i2}$ activation.** Nef inhibits chemoattractant-mediated calcium flux in Jurkat cells (*A1*) and the U937 cell line (*A2*). Cells were co-transfected with CD8 and Nef, co-expressers were purified by CD8-positive selection (Stem Cell Technologies), and Nef effect in Jurkat cells was evaluated by measuring cell surface CD4 expression. The time course of CXCL12 (10 nM)-initiated calcium flux profiles was obtained using FlexStation III and the recommended assay. Results are representative of four experiments. Agonist (CXCL12 followed by CCL2) dose (10 or 100 nM)-response profiles of intracellular calcium flux in U937 transfectants were analyzed by fluorescence ratiometry in a PTI fluorimeter (33). *B1*, time course of CXCL12-initiated Ca^{2+} flux in HeLa cells expressing CerFP or Nef-CerFP (*red*) was monitored by video capture at 30 frames/s of Fluo-4 emission (*green*) up to 150 s after CXCL12 addition. The *arrows* denote CerFP or Nef-CerFP cells (expressed at ~10–15% efficiency around 12–16 h post-transfection) to highlight their difference in Fluo-4 intensity. Fluorescent data were collected from ~10 ROIs for each field, the calcium flux was measured in >5 fields for each condition in an experiment, and the experiments were repeated three times ($n = 50–60$). The change in the intensities was analyzed using the Leica software followed by graphing using EXCEL. Ca^{2+} flux profiles of a few (to avoid clutter) representative cells (ROIs) expressing CerFP (*left*) or Nef-CerFP (*right*) are shown in *B2*, with the *ordinate* showing relative intensity of Fluo-4 emission. CXCL12-initiated Ca^{2+} flux is profiled in purified CEM cells co-transfected with CD8 and WT, null, or other Nef mutants. CEM cells were transfected with CD8, WT, null, or the indicated Nef mutants, and CD8(+) cells were purified prior to measurement of Ca^{2+} flux (as described above) (*B3*). Nef expression enhanced cAMP levels under basal conditions or after $G\alpha_s$ activation by isoproterenol (*C*) or by forskolin stimulation of adenylyl cyclase (*D*). However, Nef did not further enhance the cAMP levels after isoproterenol treatment with transfectants overexpressing $G\alpha_{i3}$ (*E*). Jurkat cells were cotransfected with CD8 and Nef or vector (for *C–E*) and with a $G\alpha_{i3}$ expression plasmid (only for *E*). Transfected cells were purified by CD8 selection and assayed for cAMP production as described under "Experimental Procedures" ($n = 4$; *error bars* represent S.E.; *, $p < 0.05$).

chambers counted in a cell sorter after the addition of a known number of fluorescent reference particles (Spherotech, Inc., Libertyville, IL) (38). Flow cytometric detection of F-actin by phalloidin staining has been described (38).

Statistical Analyses—The statistical analyses were performed using GraphPad Prism version 5.0. A paired *t* test or one-way analysis of variance test was performed as appropriate, to determine the significance of the observed differences between the paired or unpaired samples. A value of $p < 0.05$ was considered to be significant in all of the analyses. The graphs were generated using either Microsoft Excel or GraphPad Prism, and the *bars* represent mean ± S.E.

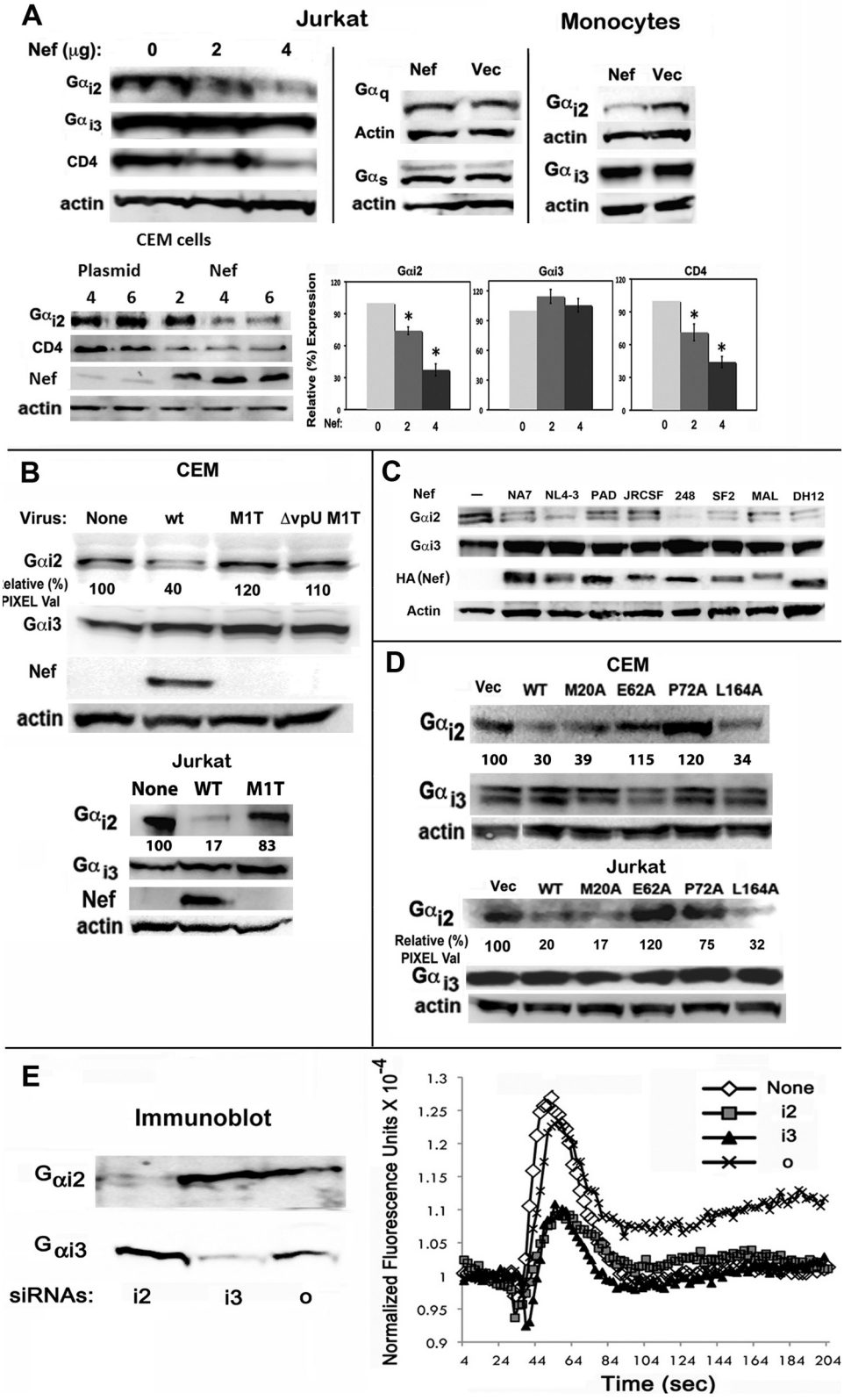

RESULTS

Nef-induced Chemotaxis Defect in T Cells and Monocytes—Nef has been shown to impair chemotaxis toward CXCL12 in lymphoid cell lines, presumably through mechanisms other than depletion of cell surface CXCR4 (24, 25, 29, 39, 40). To investigate how Nef subverts chemotactic responses downstream of chemokine receptors, we selected cells for study in which Nef only modestly (<50%) reduced receptor expression. These included the T cell lines, CEM and Jurkat, human peripheral blood mononuclear cells (PBMCs), and human monocytes. Despite the relatively modest reduction in receptor levels (data not shown), Nef expression still markedly inhibited CXCL12-, CCL19-, CCL2-, or formylmethionylleucylphenylalanine-induced chemotaxis (Fig. 1, *A–C*).

The inhibition occurred irrespective of whether Nef was expressed by DNA transfection (Fig. 1, *A1–A4*, *B* (*right two panels*), and C (*right panel*)), protein transduction of monocytes (Fig. 1*C*, *left panel*), or single cycle HIV infection (Fig. 1*B*, *left panel*). Alanine substitutions disrupting the Nef polyglutamic motif at position 62 (E62A), the P*XX*P motif at 72 (P72A), or alanine substitutions at threonine 162 (T162A) and at histidine 166 (H166A) partially or completely reversed the inhibitory effect (Fig. 1, *A3* and *A4*). The chemotactic defect corresponded to the marked reduction of F-actin accumulation in response to CXCL12 or CCL2 in Nef-expressing Jurkat cells, monocytes, and PBMCs (Fig. 1*D*).

Nef Markedly Inhibited Biochemical Readouts of Early G-protein Signaling from Agonist-stimulated Chemokine Receptors—Most, if not all, chemokines activate Gα$_i$-coupled GPCRs. An agonist-bound GPCR exchanges GTP for GDP in the Gα subunit of receptor-bound heterotrimeric G-protein. This results in Gα and Gβγ dissociation and the activation of downstream effectors. First, we examined the immediate consequence of Gβγ dissociation by monitoring intracellular Ca^{2+} flux from ER stores mediated by inositol 1,4,5-trisphosphate in response to activation of phospholipase C. We found that Nef expression markedly attenuated the rapid chemokine-induced mobilization of intracellular Ca^{2+} normally observed in Jurkat cells and abolished the response in U937 cells (Fig. 2, *A1* and *A2*). We also visualized single cell Ca^{2+} flux in response to CXCL12 stimulation of HeLa cells expressing either Cerulean fluorescent protein (CerFP) or Nef-CerFP by real-time time lapse confocal video microscopy. CXCL12 increased intracellular Ca^{2+} in the CerFP-expressing cells, but not the Nef-CerFP cells (Fig. 2, *B1*). This was confirmed by quantitative kinetic analysis of Ca^{2+} flux of individual cells expressing CerFP or Nef-CerFP (Fig. 2, *B2*). These data suggested that Nef might perturb chemokine-mediated G-protein dissociation from cognate GPCR(s). In agreement with the corresponding effects on chemotaxis, alanine substitutions of four glutamates at 62 and at the P*XX*P motif partially reversed the Nef-induced inhibition of CXCL12-mediated calcium release from the ER (Fig. 2, *B3*).

Next, we inquired whether Nef subverted activation of G-protein α subunit(s). The major effectors of activated Gα$_i$ subunits are adenylyl cyclase isoforms. GTP-bound Gα$_i$ directly inhibits specific adenylyl cyclase isoforms, thereby reducing cAMP production by direct (by agents like forskolin) or hormone-induced (via activated Gα$_s$ subunit) activation of adenylyl cyclase. Basal intracellular cAMP levels reflect a steady-state equilibrium of tonic inhibition and stimulation of adenylyl cyclase isoforms by activated Gα$_i$ and Gα$_s$ subunits, respectively. We found that Nef-expressing Jurkat cells had a 2-fold higher basal cAMP level than did the null expression controls, consistent with a loss of constitutive Gα$_i$ signaling. Furthermore, Nef expression was associated with enhanced cAMP production in Jurkat cells treated with the β-adrenergic agonist, isoproterenol (*ISOPRO*), or forskolin, a direct adenylyl cyclase activator (Fig. 2, *C* and *D*). However, basal or hormone-induced cAMP levels were not enhanced in Nef(+) cells co-expressing recombinant Gα$_{i3}$ (Fig. 2*E*). This suggested that Nef might solely target Gα$_{i2}$ because Jurkat cells and lymphocytes express Gα$_{i2}$ and Gα$_{i3}$, not Gα$_{i1}$.

Nef Induced a Marked Loss of Steady-state Levels of Gα$_{i2}$ but Not Gα$_{i3}$ or Other Gα Subunits—To determine if Nef impaired G-protein functionality or induced a physical loss or sequestration of one or more G-protein subunits, we quantified the steady-state levels of Gα subunits in Nef(+) cells by immunoblotting. We found that Nef induced a dose-dependent decrease in Gα$_{i2}$ levels in Jurkat/CEM cells and monocytes, comparable in magnitude with CD4 down-regulation in Jurkat or CEM cells (Fig. 3*A*). In contrast, Gα$_{i3}$ in Jurkat cells, CEM cells (not shown), and monocytes or Gα$_q$ and Gα$_s$ in Jurkat cells were unaffected (Fig. 3*A*).

In single cycle HIV-1 infections, loss of Gα$_{i2}$ correlated with Nef expression. Gα$_{i2}$ levels were unaltered in cells infected with viruses deleted for Nef or Nef and vpU (Fig. 3*B*). Eight different HIV-1 Nef alleles induced a specific loss of Gα$_{i2}$ of comparable magnitude (Fig. 3*C*). The differences in the level of down-regulation might be dependent on critical Nef residues, and they are a subject of further investigation. Gα$_{i2}$ levels were unaffected in cells expressing Nef mutants with alanine substitutions in the acidic motif at 62 (E62A) or in the polyproline motif

FIGURE 3. **Biochemical and genetic analysis of Nef induced loss of steady-state levels of Gα$_{i2}$ subunit in Jurkat and CEM cell lines and primary human monocytes in the context of DNA transfection or single cycle HIV infection.** *A*, cellular extracts were immunoblotted for Gα$_{i2}$, Gα$_{i3}$, Gα$_q$, Gα$_s$, CD4, or actin. Protein bands were scanned for pixel density, and results are plotted as histograms with *error bars* representing S.E. ($n = 3$; *, $p < 0.03$). *B*, loss of Gα$_{i2}$ in single cycle infections of CEM/Jurkat cells with identical reverse transcriptase unit equivalents of VSV-G pseudotyped Nef$^+$ (*wt*), but not Nef$^-$ (*M1T*) or Nef$^-$vpU$^-$ (Δ*vpU M1T*) NL4-3 HIVs expressing murine CD4 antigen in place of vpR. Gα$_{i2}$, Gα$_{i3}$, and Nef were detected by immunoblotting cellular extracts. *C*, HIV-1 Nef alleles induced a specific loss of Gα$_{i2}$ of comparable magnitude. Jurkat cells were transfected with various Nef alleles, and the levels of Gα$_{i2}$ down-regulation were assessed. Cellular extracts were immunoblotted for Gα$_{i2}$, Gα$_{i3}$, HA (Nef), or actin. *D*, certain Nef mutants had lost the ability to induce loss of Gα$_{i2}$. Extracts of CEM/Jurkat cells transfected with the indicated Nef derivatives were analyzed by SDS-PAGE followed by immunoblotting for actin, Gα$_{i2}$, and Gα$_{i3}$. Relative pixel values in *B* and *C* represent averages from two experiments for each case. *E*, knockdown of Gα$_{i2}$ or Gα$_{i2}$ by cognate siRNAs partially inhibited CXCL12-dependent calcium flux. Jurkat cells were co-transfected with CD8 and Nef or an empty vector following siRNA nucleofection and expression for 48 h. ~2×10^2 transfectants were adjusted to reflect constant levels of CD8 and analyzed for CXCL12-initiated intracellular calcium flux. Gα$_{i2}$ and Gα$_{i2}$ in the respective siRNA transfectants were detected by immunoblotting as described above.

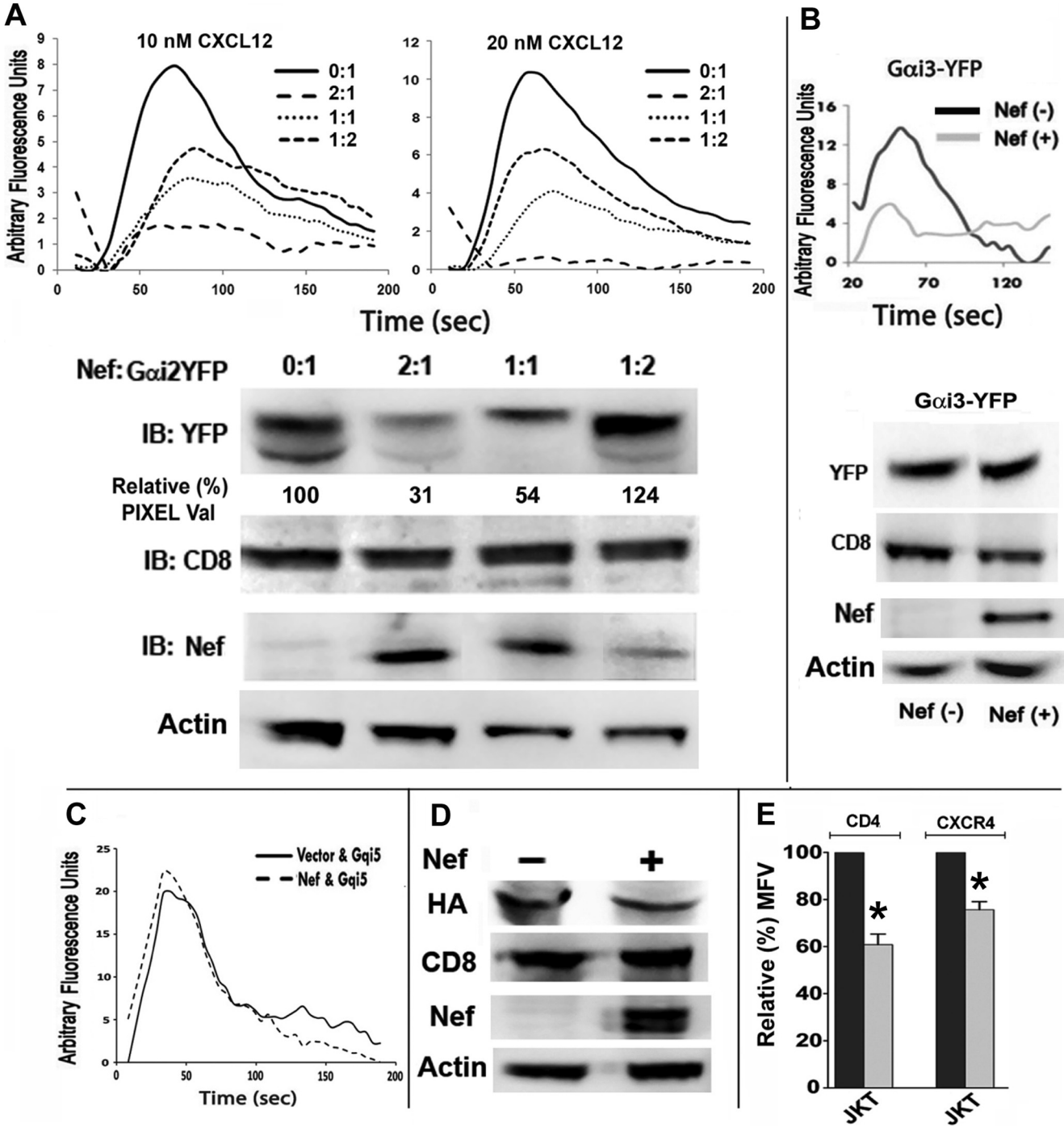

FIGURE 4. **Nef-induced inhibition of G-protein signaling and Gα$_{i2}$ degradation were partially rectified by overexpression of recombinant Gα$_{i2}$, and a Gq$_{i5}$ chimera replacing the C-terminal five residues with those of Gα$_i$ was resistant to Nef effect.** CEM cells were nucleofected with CD8 and YFP-tagged Gα$_{i2}$ (*A*) or Gα$_{i3}$ (*B*) subunits with or without a molar excess of Nef. Purified CD8 transfectants were analyzed for CXCL12-driven intracellular Ca^{2+} flux. Nef-induced loss of Ca^{2+} flux in response to CXCL12 was partially reversed in cells expressing a 2-fold molar excess of Gα$_{i2}$ over Nef (*A*), but Gα$_{i3}$ co-expression did not ameliorate Ca^{2+} flux deficit (*B*). At a 2-fold molar excess of Gα$_{i2}$ over Nef, there was much less relative loss in the steady-state levels of Gα$_{i2}$-YFP (*A*, *bottom*). There was no loss of Gα$_{i3}$-YFP with or without of Nef (*B*, *bottom*). Relative Gα$_{i2}$-YFP pixel values shown in the immunoblot are averages from three experiments. *C*, Nef did not inhibit CXCL12-initiated calcium flux in cells expressing Gq$_{i5}$ chimera replacing the C-terminal five residues with those of Gα$_{i2}$, (36). Jurkat transfectants co-expressing CD8 and Gq$_{i5}$ chimera with or without Nef were purified and analyzed as described above. *D*, Nef did not alter the stability of co-expressed Gq$_{i5}$ chimera. Cell extracts of Jurkat transfectants were analyzed for expression of HA-tagged Gq$_{i5}$, co-expressed CD8, Nef, and actin. *E*, Gq$_{i5}$ expression did not alter Nef-induced down-regulation of CD4 or CXCR4 at the PM. *Black* and *gray histograms* (with *error bars* (S.E.)) represent normalized data for CD8(−) and CD8(+) gated cells ($n = 3$; *, $p < 0.05$). *IB*, immunoblot.

at 72 (P72A) in Jurkat and CEM cells (Fig. 3*D*). We compared the effects of siRNA knockdown of individual Gα$_{i2}$, Gα$_{i3}$, or G$_o$ subunits on agonist-driven Ca^{2+} flux. Knockdown of Gα$_{i2}$ or Gα$_{i3}$ resulted in a significant (~60%) decrease in the agonist-mediated Ca^{2+} flux (Fig. 3*E*). Thus, the Nef-induced defect in early G-protein signaling reflected by chemokine-mediated Ca^{2+} flux was attributed to the physical loss of the Gα$_{i2}$ subunit.

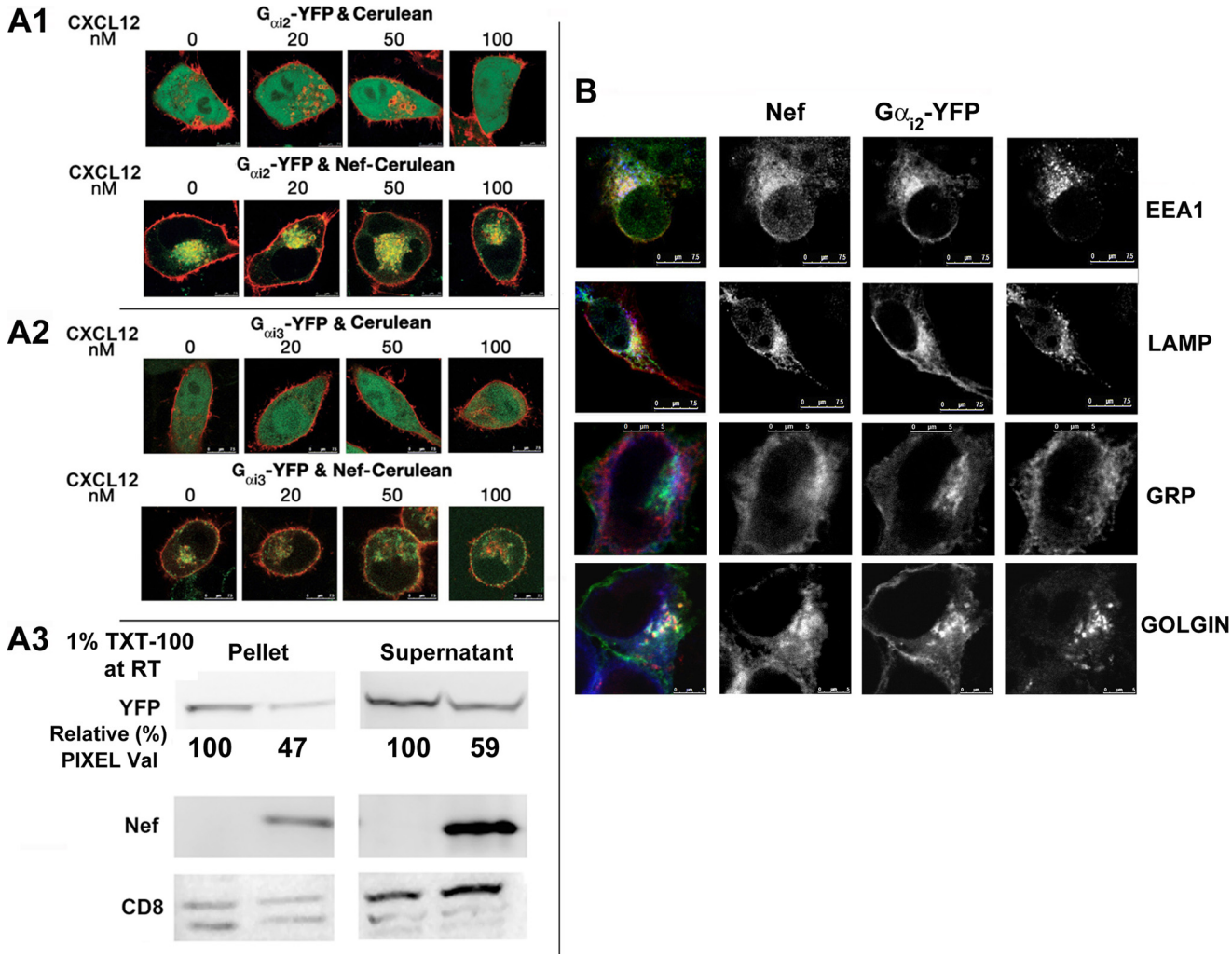

FIGURE 5. **Nef co-localized with and promoted endolysosomal sequestration of Gα$_{i2}$ but not Gα$_{i3}$.** HeLa cells in coverglass chambers were co-transfected with YFP-tagged Gα$_{i2}$ (*A1*) or Gα$_{i3}$ (*A2*) with CerFP or Nef-CerFP (*top* or *bottom row* in *A1* and *A2*) and treated for 10 min at 37 °C with increasing concentrations of CXCL12 or not before processing for live microscopy. Cerulean is *green*, and YFP is *red*. *A3*, Nef-induced loss of YFP-tagged Gα$_{i2}$ occurred irrespective of whether or not the G-protein was membrane-associated. Cells were extracted in a buffer containing 1% (w/v) Triton X-100 (*TXT-100*) at 25 °C (room temperature (*RT*)), conditions that are known to strip most if not all membrane-associated proteins. Membrane (pellet) and cytoplasmic (supernatant) extracts were resolved by SDS-PAGE followed by immunoblot detection of YFP, Nef, and CD8. Relative Gα$_{i2}$-YFP pixel values are averages from three experiments. *B*, in Nef-expressing cells, YFP-tagged Gα$_{i2}$ (*red*) co-localized with Nef-CerFP (*green*) and endolysosomal markers, EEA1 and LAMP (*blue*) proteins, but not with markers (*blue*) for ER (*GRP*) or Golgi (*GOLGIN*).

Nef-induced Inhibition of Gα$_{i2}$ Degradation Was Partially Rectified by Overexpression of Recombinant Gα$_{i2}$, and a Gq$_{i5}$ Chimera Replacing the C-terminal Five Residues with Those of Gα$_{i}$ Was Resistant to the Nef Effect—Co-expression of YFP-tagged recombinant Gα$_{i1}$ (not shown), Gα$_{i2}$, or Gα$_{i3}$ failed to restore CXCL12-mediated Ca^{2+} flux in Jurkat cells expressing a 2-fold molar excess of Nef over the recombinant Gα$_{i2}$ subunits (Fig. 4, *A* and *B*). The failure to reverse CXCL12-mediated Ca^{2+} flux by recombinant Gα$_{i2}$ reflected the destruction of endogenous and a substantial loss of the co-expressed Gα$_{i2}$ (Fig. 4*A*, *bottom*). Only by increasing the ratio of Gα$_{i2}$ to Nef expression could the signaling be partially restored. Although there was no loss of Gα$_{i3}$-YFP co-expressed with a molar excess of Nef (Fig. 4*B*, *bottom*), Gα$_{i3}$-YFP failed to restore CXCL12-initiated Ca^{2+} flux (Fig. 4*B*, *top*).

A small C-terminal region of Gα subunit(s) is the GPCR selectivity determinant and a recombinant Gq$_{i5}$, which exchanged five Gq residues at the C terminus for those of Gα$_{i2}$, thus becoming functionally equivalent to Gα$_{i2}$ in chemokine responsiveness and pertussis toxin sensitivity (36). Nef failed to alter the expression of or inhibit CXCL12-induced intracellular Ca^{2+} flux from the Gq$_{i5}$ chimera (Fig. 4, *C* and *D*) while still down-regulating CD4 and CXCR4 (Fig. 4*E*). Because heterotrimeric G-proteins are bound to the receptor in an inactive state, it is possible that the Nef-induced lysosomal sequestration of Gα$_{i2}$ reflects aberrant trafficking of CXCR4. However, this is unlikely because cells co-expressing Nef and Gq$_{i5}$ chimera retained CXCL12-driven Ca^{2+} flux.

Nef Co-localized with and Promoted Sequestration of Gα$_{i2}$, but Not Gα$_{i3}$, in the Perinuclear Region Enriched for Endolysosomal Markers—To determine whether Nef interacted with Gα$_{i2}$ *in vivo*, we examined the subcellular distribution of YFP-tagged recombinant Gα$_{i2}$ or Gα$_{i3}$ in HeLa cells co-expressing CerFP or Nef-CerFP. In the CerFP-expressing cells, Gα$_{i2}$ and Gα$_{i3}$ were distributed at the PM irrespective of CXCL12 exposure. In Nef-expressing cells, a substantial fraction of Gα$_{i2}$ co-localized with Nef in the perinuclear region (co-localization correlation of >0.75), regardless of CXCL12 treatment, whereas Gα$_{i3}$ did not co-localize

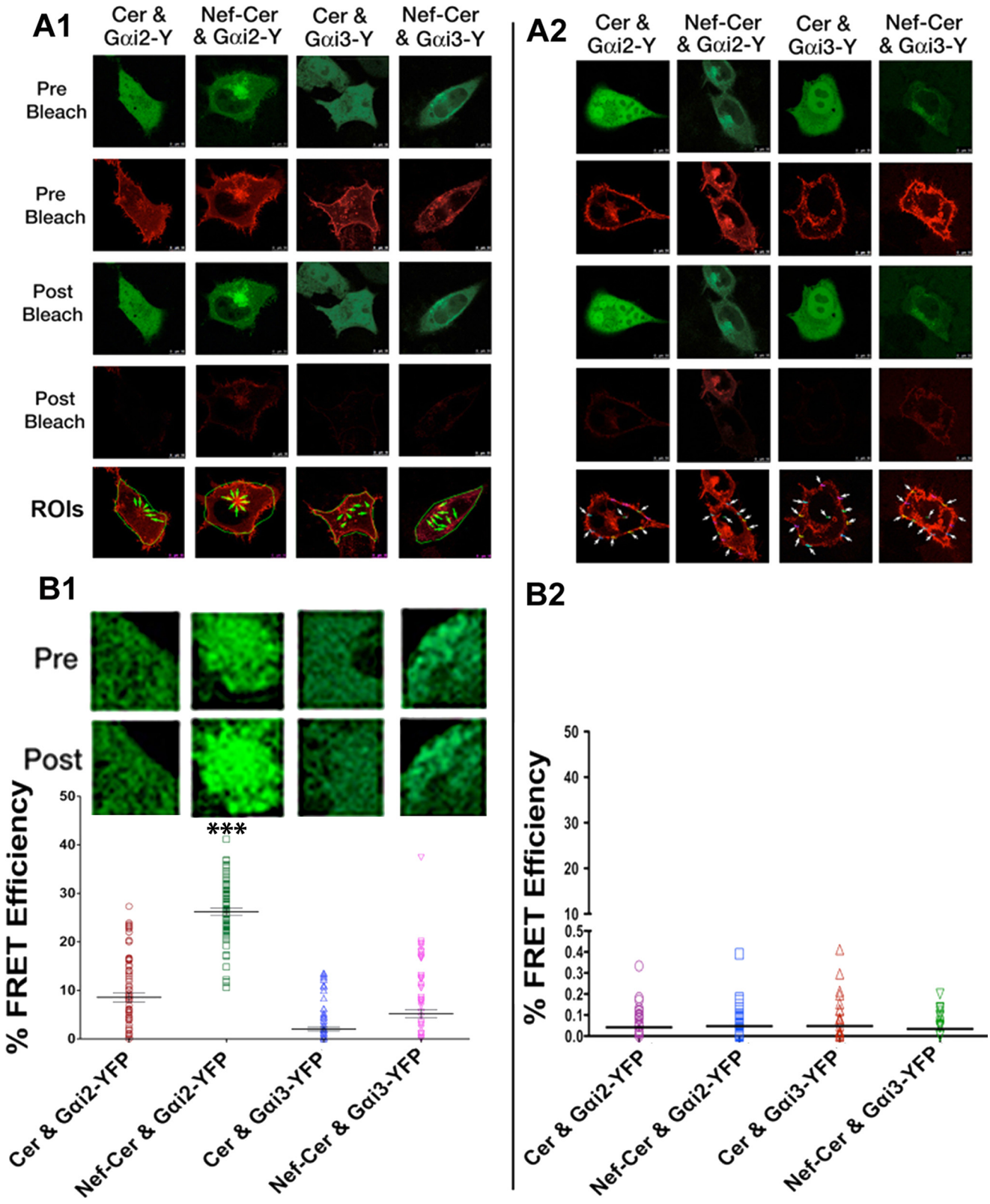

FIGURE 6. **Nef associated with Gα$_{i2}$ but not Gα$_{i3}$ *in vivo*.** Acceptor photobleaching FRET assay of HeLa cells co-expressing CerFP or Nef-CerFP with YFP-tagged Gα$_{i2}$ or Gα$_{i3}$. FRET assay was limited to Gα$_{i2}$ or Gα$_{i3}$ with CerFP or Nef-CerFP in the perinuclear area (*A1*) or at the PM (*A2*). Photomicrographs are representative of 10 fields (cells). Fluorescence intensities of 10 ROIs (*arrows*) corresponding to Gα$_{i2}$ or Gα$_{i3}$ in the perinuclear regions (*B1*) or at the PM (*B2*) in each cell were examined before (*Pre*) and after (*Post*) photobleaching, and calculated FRET efficiencies for all ROIs (~100) from three independent experiments are shown as scatter plots with *error bars*. Donor emission of representative ROIs pre- and postphotobleaching is shown in the *inset above* the graph. The calculated statistical significance is represented (*, $p < 01$).

with Nef (correlation of <0.04) (Fig. 5, *A1* and *A2*). Nef expression resulted in an equivalent loss of membrane-associated *versus* detergent-soluble fractions of Gα$_{i2}$-YFP, indicating that Nef induced collective loss of Gα$_{i2}$ inside the cell (Fig. 5, *A3*). The Gα$_{i2}$- and Nef-containing vesicular structures stained positively for endolysosomal markers EEA1 and LAMPs but not with the markers for ER (GRP) or Golgi (Golgin) (Fig. 5*B*).

Nef-mediated Lysosomal Sequestration of Gα$_{i2}$ Reflected in Vivo Interaction of Nef and Gα$_{i2}$—Next, we performed live FRET microscopy to analyze nearest neighbor interactions between Nef and Gα$_{i}$. We measured FRET efficiency on the basis of the increase in the donor (CFP or Nef-CFP) fluorescence upon photobleaching the YFP-tagged Gα$_{i2}$ acceptor. FRET efficiencies generated by tandem CFP-YFP fusion protein served as the positive control. We analyzed >10 cells in each of three experiments, and photomicrographs of one representative cell are shown (Fig. 6, *A1*), with the calculated FRET efficiencies of ~100 ROIs shown in the graphs *below* (Fig. 6, *A2*). There was substantial FRET between Nef-CFP and Gα$_{i2}$-YFP at the intracellular, perinuclear region (Fig. 6, *B1*) but not at the PM (Fig. 6, *B2*) or anywhere in the cell with Gα$_{i3}$-YFP (Fig. 6, *B1* and *B2*).

Nef Interacted with Gα$_{i2}$ in Vitro and Induced Gα$_{i2}$ Ubiquitination—To confirm the physical interaction between Nef and Gα$_{i2}$, we performed *in vitro* GST pull-down assays of leukocyte extracts using GST or GST-Nef. Using extracts from Jurkat T-cells and primary monocytes, we found that GST-Nef bound Gα$_{i2}$ but not Gα$_{i3}$ in a dose-responsive manner (Fig. 7*A*).

To inquire whether the loss of Gα$_{i2}$ was a consequence of Nef-induced ubiquitination of Gα$_{i2}$ and its subsequent lysosomal proteolysis, we directly evaluated whether Gα$_{i2}$ was ubiquitinated. We co-transfected CEM cells with vectors expressing FLAG-tagged ubiquitin and either Nef or control. Nef expression resulted in significant loss of Gα$_{i2}$ (Fig. 7, *B1* (*left*)). Cellular extracts were immunoprecipitated with FLAG mAb-coated beads, and the selected proteins were immunoblotted for Gα$_{i2}$ using mouse monoclonal antibody (Fig. 7, *B1* (*right*)) or rabbit polyclonal antibody (Fig. 7, *B2*). Nef expression resulted in significant loss of Gα$_{i2}$ (Fig. 7*B*, *left*). Two immunoreactive bands of ~53 and ~63 kDa were seen in lysates of Nef-expressing cells, probably representing mono- and diubiquitinated native Gα$_{i2}$ (Fig. 7*B*, *right*).

We first evaluated the effects of Dynasore (41), a small molecular weight dynamin inhibitor, and the proteosome inhibitor, epoxomycin. We found that pretreatment with the inhibitors substantially reversed the Nef-induced loss of Gα$_{i2}$ (Fig. 7*C*).

Nef Co-localizes with E3 Ubiquitin Ligases AIP4 and Nedd4—Ubiquitination of agonist-occupied CXCR4 by the Nedd4-like E3 ubiquitin ligase AIP4 (42) primes it for traffic through the ESCRT pathway, ultimately resulting in lysosomal proteolysis (43, 44). We inquired whether Nef-induced endolysosomal trafficking of Gα$_{i2}$ was facilitated by these E3 ligase(s). We stained HeLa cells co-transfected with plasmids expressing YFP-tagged Gα$_{i2}$ or Gα$_{i3}$ and Nef-CerFP or CerFP with antibodies against AIP4 or NEDD4. There was extensive co-localization of Gα$_{i2}$ with Nef and AIP4 in the perinuclear area (Fig. 8*A*). There was a similar co-distribution of Nef and Gα$_{i2}$ with the NEDD4-positive region (Fig. 8*B*). In contrast, Gα$_{i3}$ was mostly at the PM, with no evidence of co-localization with Nef, AIP4, or NEDD4 (Fig. 8, *A* and *B* (*bottom*)).

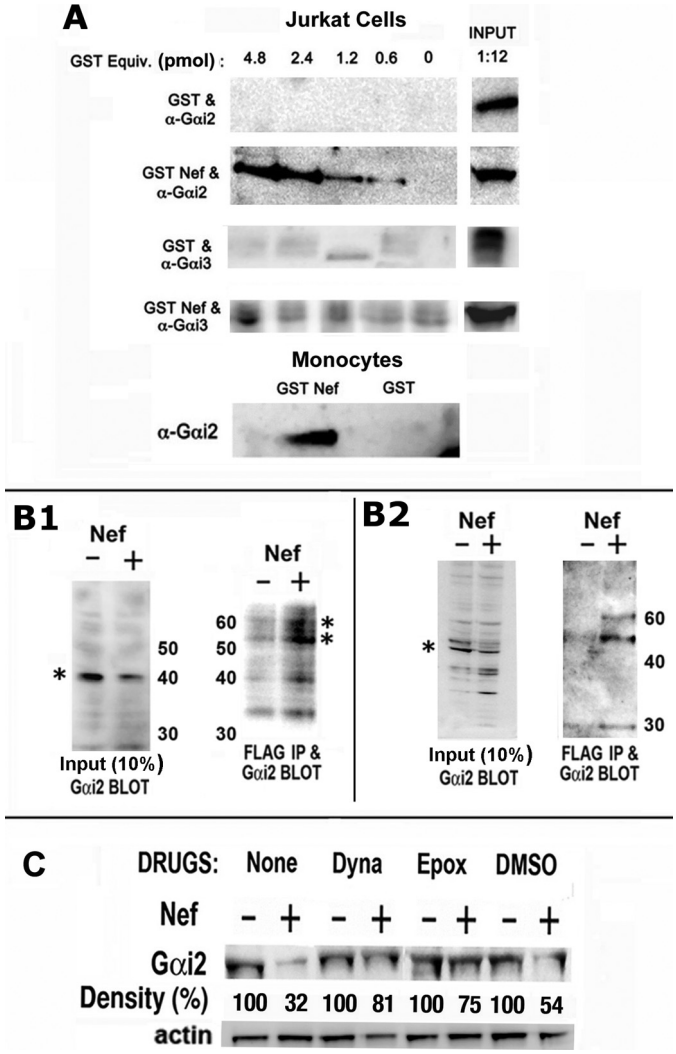

FIGURE 7. **Nef interacted with Gα$_{i2}$ *in vitro* and induced Gα$_{i2}$ ubiquitination.** *A*, varying amounts of purified GST or GST Nef were incubated with cellular extracts of Jurkat cells or human monocytes. Bound proteins were resolved by SDS-PAGE, and Gα$_{i}$ species were detected by immunoblotting. *B*, Nef-induced ubiquitination of native Gα$_{i2}$ in Nef-expressing CEM cells. CEM cells were co-transfected with FLAG-tagged ubiquitin and Nef or null plasmid. Cellular extracts were directly immunoblotted for Gα$_{i2}$ (*B1* and *B2*, *left panels*) or immunoprecipitated first with anti-FLAG polyclonal antibody (*B1*) or mAb (*B2*) followed by immunoblotting for Gα$_{i2}$. *Asterisks* denote Gα$_{i2}$ (*left*) and mono- and diubiquitinated Gα$_{i2}$ (*right*). *Numbers* (kDa) refer to molecular mass markers. Data are representative of three experiments. *C*, Nef-mediated Gα$_{i2}$ breakdown was partially rectified by Dynasore, a small molecular weight inhibitor of dynamin, or the proteosome inhibitor epoxomycin. Cellular extracts were analyzed by immunoblotting for Gα$_{i2}$. Gα$_{i2}$ bands are shown pairwise for Nef(+) *versus* Nef(−) for each treatment with relative (%) density (average values from three experiments) denoted *below*.

AIP4 Bound Gα$_{i2}$ through the HECT Domain of the E3 Ligase and to the Tetraglutamate and Polyproline Motif of Nef, Presumably through the WW Domain(s)—We evaluated the binding potential of AIP4 for Nef and Gα$_{i}$ subunits *in vitro* and *in vivo*. In GST-Nef pull-down assays, AIP4 was recovered from Jurkat cell extracts in a specific and quantifiable manner (Fig. 9*A*, *top*). Like other members of the NEDD4 family of HECT domain E3 ligases, AIP4 has four WW domains (Fig. 9*A*, *center*), which preferentially bind to proline-rich PY motifs (45–47) or hyperphosphorylated C termini of PM receptors (44). Accordingly, GST-AIP4 bound poorly to Nef mutants with sub-

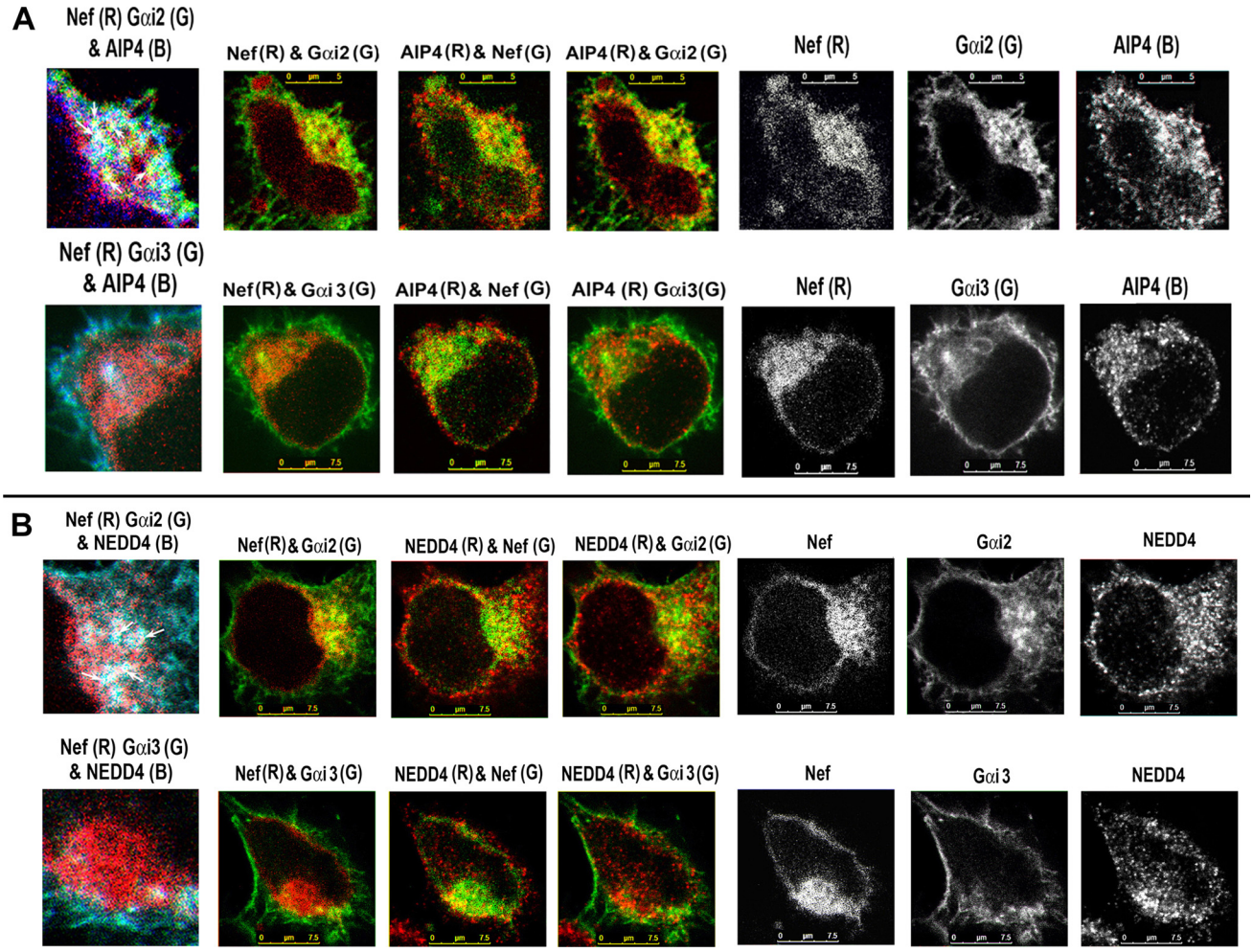

FIGURE 8. **Nef recruits HECT domain E3 ligases, AIP4, or NEDD4 and facilitates Gα$_{i2}$ ubiquitination, presumably as a ternary complex.** *A*, Nef co-localized with Gα$_{i2}$ but not with Gα$_{i3}$ in the AIP4-enriched perinuclear region. HeLa cells co-transfected with Nef-CerFP and YFP-tagged Gα$_{i2}$ or Gα$_{i3}$ were fixed, permeabilized, and stained with murine mAb against AIP4 followed by Alexa 647-conjugated anti-mouse IgG. *B*, Nef co-localizes with Gα$_{i2}$ but not Gα$_{i3}$ in NEDD4-positive regions in HeLa cells. Experimental details are as above except for the use of rabbit polyclonal antibody against NEDD4. Monochromatic images on the *right* in each *row* correspond to Nef-CerFP, YFP-tagged Gα$_{i2}$ or Gα$_{i3}$, and anti-AIP4 or -NEDD4 fluorescence with two-channel (like AIP4/NEDD4 and Gα$_{i2}$ or AIP4/NEDD4 and Nef, etc.) composite images shown on the *left*. 4× cropped RGB images (Nef-CerFP (R), Gα$_{i2}$- or Gα$_{i3}$-YFP (G), and AIP4/NEDD4 (B)) with *arrows* denoting vesicles showing maximal co-localization are shown on the *far left* in each *row*.

stitutions of the polyglutamate at position 62 (E62A) or the polyproline tract at position 72 (P72A) (Fig. 9*A*, *bottom left*). GST fusion proteins containing WT AIP4 or a deletion mutant that excised all four WW domains but retained the HECT domain bound Gα$_{i2}$ (Fig. 9A, *bottom right*).

Next, we co-transfected Jurkat cells with expression vectors for FLAG-AIP4 and Nef-HA or a control plasmid. Immunoblotting FLAG immunoprecipitates prepared from lysates from co-expressing cells for Nef-HA revealed an interaction between them (Fig. 9*B*, *top*). Furthermore, mutations at the Nef motifs judged to be critical for *in vitro* binding to AIP4 were also impaired for *in vivo* binding (Fig. 9, *B* (*bottom*) and *C*).

From these observations collectively, we concluded that Nef facilitated Gα$_{i2}$ ubiquitination by recruitment of the NEDD4 class of HECT domain E3 ligases, presumably as a ternary complex of Nef, Gα$_{i2}$, and E3 ligases(s).

Nef-induced Loss of Gα$_{i2}$ Was Partially Reversed by Expression of Enzymatically Defective AIP4 or by siRNA Knockdown of AIP4 or NEDD4—To firmly establish the role of AIP4 in the Nef-induced Gα$_{i2}$ ubiquitination and degradation, Jurkat cells were co-transfected with Nef or an empty vector and WT or an enzymatically defective HECT domain mutant, AIP4-C830A (43, 48). AIP4-C830A overexpression reversed the Nef-mediated loss of Gα$_{i2}$ (Fig. 10*A*).

We then compared the effect of siRNA knockdown of AIP4 or NEDD4 on Nef-induced loss of endogenous Gα$_{i2}$ in Jurkat and CEM cells. siRNA-induced reduction of AIP4 or NEDD4 E3 ligase reversed the Nef-induced Gα$_{i2}$ loss (Fig. 10*B*). Simultaneously, we evaluated chemotaxis of Nef *versus* non-Nef transfectants after siRNA knockdown of AIP4 or NEDD4. Nef-mediated chemotactic inhibition was partially rectified by NEDD4 knockdown, although not nearly as well as by the AIP4 knockdown (Fig. 10*C*). Silencing the E3 ligases did not affect cell viability or curtail other activities of Nef, such as CD4 (Fig. 10*D*) down-regulation.

Lysine at Position 296 Is the Critical Determinant of Gα$_{i2}$ Ubiquitination and Degradation in Nef-expressing Cells—Finally, we identified the potential lysine residue in Gα$_{i2}$ that may be targeted for ubiquitination by AIP4 in Nef-expressing cells,

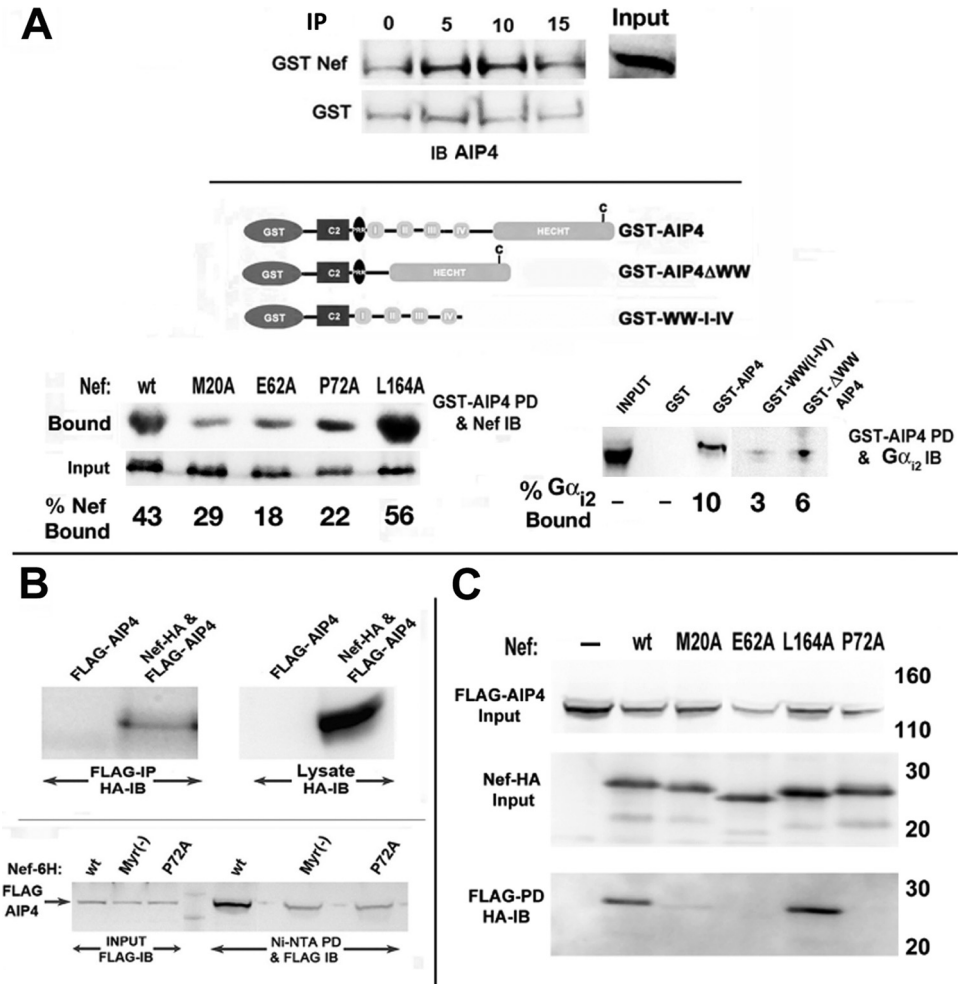

FIGURE 9. **Biochemical and genetic analysis of Nef interaction *in vivo* with Gα$_{i2}$ and E3 ligases.** *A*, Nef and Gα$_{i2}$ interacted with AIP4 *in vitro*. Shown is a schematic illustration (*top*) of GST-tagged WT AIP4 and mutants deleted for the WW or HECT domains (44). Jurkat cells were transfected with WT, M20A, E62A, P72A, or L164A Nef mutant, and cellular extracts were incubated with ~22 pmol of GST or GST-AIP4 immobilized on agarose beads. GST-bound fractions and unselected lysate (2%) were analyzed for Nef by immunoblotting (*left*). Cellular extracts of Jurkat cells were reacted with equimolar amounts (~22 pM) of GST-AIP4, GST-AIP4 ΔWW, GST-WW-I-IV, or GST alone. Bound fractions were analyzed by immunoblotting with anti-Gα$_{i2}$ mAb (*right*). *Input*, an aliquot of extract immunoblotted without selection. *Numbers* in both cases refer to bound fraction (%) averaged from two experiments. *B*, *in vivo* interaction of Nef with AIP4. Extracts of Jurkat cells cotransfected with FLAG-AIP4 and HA-tagged Nef or empty HA vector and immunoprecipitated with FLAG-mAb and Nef were identified by immunoblotting with rabbit anti-HA (*top*). Relative binding affinity of Nef mutants for AIP4 was evaluated in Jurkat cells cotransfected with GFP, FLAG-AIP4, and His$_6$-tagged WT or mutant Nef (*bottom*). Cellular extracts were bound to Ni^{2+}-nitrilotriacetic acid beads, and the bound FLAG-AIP4 was detected by immunoblotting with anti-FLAG mAb. *C*, alternatively, Jurkat cells were cotransfected with GFP, FLAG-AIP4, and HA-tagged WT or mutant Nef. Extracts were immunoprecipitated with FLAG mAb, followed by immunoblotting with HA antibody. Data represent results from three experiments.

by evaluating the susceptibility to Nef of individual Gα$_{i2}$-YFP mutants that exchanged unique lysines for arginines at positions 296, 307, and 314. Jurkat cells were co-transfected with wild type or the respective LYS/ARG mutants with or without Nef. Immunoblotting for YFP showed that the LYS/ARG mutant, M1, was resistant to Nef-induced steady-state loss (Fig. 11*A*). In agreement, CXCL12-driven Ca^{2+} flux in M1 mutant-expressing cells was relatively more resistant than in the WT Gα$_{i2}$-YFP expressers (Fig. 11*B*). We then examined the subcellular distribution of WT Gα$_{i2}$-YFP *versus* the M1 mutant in HeLa cells co-expressing CerFP or Nef-CerFP. In the CerFP-expressing cells, WT and M1 were distributed at the PM. In Nef-expressing cells, a substantial fraction of WT but not M1 co-localized with Nef in the perinuclear region (co-localization correlation of >0.75 *versus* <0.125) (Fig. 11*C*).

DISCUSSION

Through multiple criteria, we have shown here that HIV Nef impairs G-protein signaling from chemokine receptors by selectively targeting Gα$_{i2}$ for ubiquitination and rapid endolysosomal destruction. Nef-induced loss of steady-state levels of Gα$_{i2}$ was observed in many cell types in the context of gene transfection, HIV infection, or Nef protein transduction. Lys/Arg substitution at each of the three unique lysines near the C terminus of Gα$_{i2}$ identified lysine at 296 as the crucial determinant of Nef-induced degradation. Nef-mediated loss of Gα$_{i2}$ was shown to be dependent on ubiquitination by AIP4, because it was reversed by overexpression of catalytically defective C830A AIP4 mutant, by siRNA knockdown of AIP4, or by use of proteosomal inhibitors or a dynamin antagonist. Previous reports have shown that, following agonist activation, CXCR4 is ubiquitinated by the NEDD4 class HECT domain E3 ubiqui-

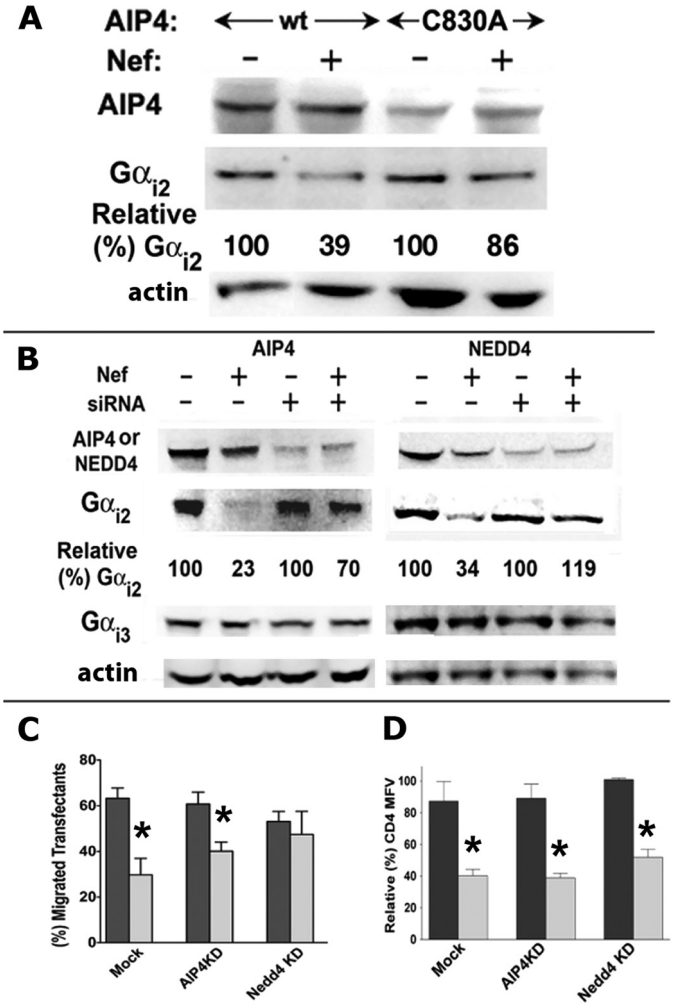

FIGURE 10. **Nef-induced loss of Gα$_{i2}$ was partially reversed by enzymatically defective AIP4 or by siRNA knockdown of AIP4 or NEDD4.** *A*, the HECT domain mutant of AIP4 (C830A) reversed Nef-induced degradation of Gα$_{i2}$. Jurkat cells were nucleofected with CD8, FLAG-tagged WT, or C830A AIP4 mutant and HA-tagged Nef or empty HA vector. Extracts from cells adjusted for equivalent CD8 expression were analyzed by immunoblotting using mAb against Gα$_{i2}$ and anti-FLAG antibody for detecting AIP4. *Numbers* refer to relative (%) Gα$_{i2}$ amounts for the respective transfectants adjusted for equivalent CD8 expression. *B*, Nef-induced loss of Gα$_{i2}$ was partially reversed by siRNA knockdown of AIP4 or NEDD4. Transfected Jurkat cells were disrupted in 0.5 ml of lysis buffer, and extracts were resolved by SDS-PAGE followed by immunoblotting for actin, NEDD4, AIP4, Gα$_{i2}$, or Gα$_{i3}$. *Numbers* denote relative (%) pixel densities of Gα$_{i2}$ averaged from three experiments. *C*, siRNA knockdown of AIP4 or NEDD4 partially reversed Nef-induced inhibition of chemotaxis toward CXCL12. After a 48-h treatment with the respective siRNAs, Jurkat cells were cotransfected with GFP and Nef(−) or Nef(+) plasmid. Cells were evaluated for chemotaxis toward 20 nM CXCL12. Histograms represent pairwise comparison of relative (%) chemotaxis efficiency of GFP(+) Nef(−) *versus* Nef(+) ($n = 3$). *D*, siRNA knockdown of AIP4 or NEDD4 did not interfere with Nef-mediated CD4 down-regulation. Jurkat cell transfectants were analyzed for CD4 expression by flow cytometry. Relative (%) CD4 mean fluorescence values for Nef(+) and Nef(−) transfectants are plotted pairwise for each condition as histograms (with *error bars*). The mean fluorescence value for Nef(−) cells in each case was arbitrarily assigned as 100 ($n = 3$); *, $p < 0.05$ when compared with their respective plasmid (mock)-transfected controls.

tin ligase AIP4 (but not NEDD4), which primes it for traffic through the ESCRT pathway, resulting in lysosomal proteolysis (43, 44). Nef recruits either E3 ligase for Gα$_{i2}$ ubiquitination without need for agonist treatment.

Nef bound Gα$_{i2}$ much better than other Gα species *in vitro*. Given the level of sequence homologies among Gα$_i$ isoforms, it is not surprising that Nef bound to Gα$_{i3}$ at 4.8 pM concentration. But it occurred at relatively much higher concentrations of Gα$_{i3}$ compared with Gα$_{i2}$, indicating that Nef preferably binds to Gα$_{i2}$ rather than Gα$_{i3}$. We repeated the experiment with increasing concentration of GSTNef, and we found binding of Gα$_{i3}$ to Nef (data not shown). But this occurred at a concentration that is physiologically not relevant. Nef and Gα$_{i2}$ co-localized *in vivo* in perinuclear vesicles enriched for endolysosomal markers, which was further validated by increased FRET intensity between Nef-CFP and Gα$_{i2}$-YFP in the intracellular vesicular structures. There was also extensive co-localization of Nef with Gα$_{i2}$ (but not Gα$_{i3}$) and AIP4 (or NEDD4) in the same perinuclear vesicles. Taken together, these findings strongly implied that Nef-induced Gα$_{i2}$ ubiquitination occurs in a ternary complex of Nef, E3 ligase, and Gα$_{i2}$. AIP4 binding to substrates is mediated by its WW domain, which targets polyproline motifs like PPPY or PPXY (47, 49, 50) or phosphothreonine and phosphoserine residues (51). Our studies showed that AIP4 bound Gα$_{i2}$ through the HECT domain and Nef, presumably through the WW domain(s). Accordingly, AIP4 poorly bound Nef mutants that substituted the polyglutamate at 62 (E62A) or the polyproline tract at position 72 (P72A). This suggested that the Src homology 3 binding domain of Nef, with the P*XX*P motif, which has been demonstrated to be important for viral replication (52, 53), might be crucial for the down-regulation of Gα$_{i2}$. Additional residues surrounding the P*XX*P motif have been shown to affect the HIV replication and disease progression (54) and might account for the variation in the ability of various Nef alleles to down-regulate Gα$_{i2}$.

Ubiquitin-dependent degradation of G-proteins(s) was originally shown for the yeast Gpa1, a Gα equivalent (55–57), which was routed to multivesicular bodies for proteolysis. Mammalian Gα$_o$ (58), Gα$_i$ (59, 60), Gα$_s$ (61, 62), and Gβγ (63, 64) subunits are presumed to be regulated by the proteasomal pathway; however, only Gα$_s$ (61, 62), transducin Gβγ (64), and Gγ$_2$ (63) were shown to be ubiquitinated. To our knowledge, Nef-induced Gα$_{i2}$ loss represents the first instance where ubiquitination routes the G-protein for endolysosomal proteolysis. A systematic analysis of essential genes in yeast important for regulating G-protein signaling identified a preponderance of genes involved with protein degradation (65). Our results indicate that mammalian cells must also carefully control expression of the essential components in the G-protein signaling pathway and that HIV Nef has probably co-opted this mechanism that regulates Gα$_{i2}$ stability.

It was of interest that, although Nef spared Gα$_i$ isomers other than Gα$_{i2}$, early G-protein signaling and chemotaxis defects perpetrated by Nef implied that other Gα$_i$ isomers were not recruited for signaling in the different cell types we have used. This was further confirmed by siRNA knockdown of either Gα$_{i2}$ or Gα$_{i3}$, which resulted in a significant (~60%) decrease in the agonist-mediated Ca^{2+} flux. Notwithstanding the paramount role(s) of Gα$_i$ in immune cell trafficking, chemokine receptors can couple to other G-proteins to facilitate chemotaxis (66–68) in monocyte/macrophages. In addition, an alternative chemokine receptor pathway has been described for certain receptor/cell combinations in dendritic cells and neutrophils (69, 70) that is activated by Gα$_{i2}$ but was dependent on G$_q$ proteins for optimal G-protein signaling and chemotaxis.

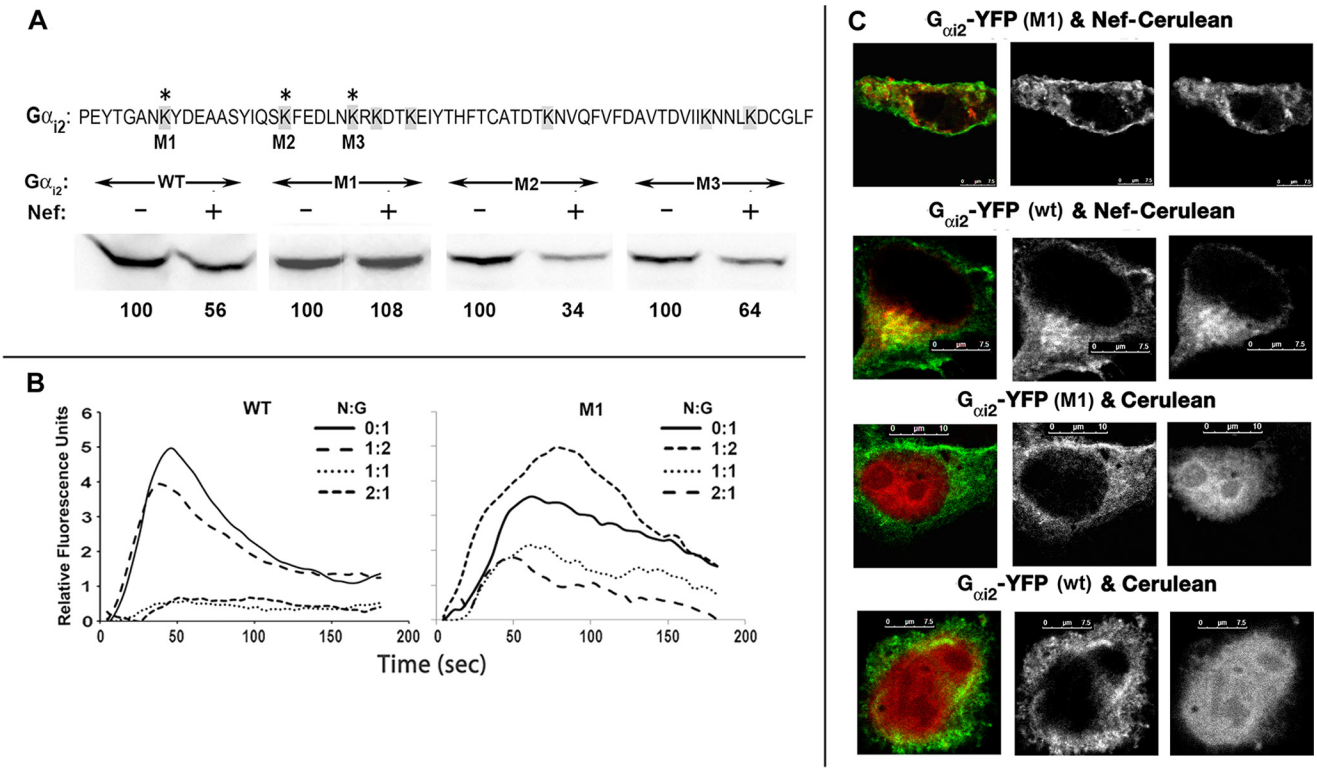

FIGURE 11. **Lysine at position 296 of Gα$_{i2}$ is the critical determinant of Nef-induced degradation.** *A*, the C-terminal 66 residues of Gα$_{i2}$ are shown at the *top*, with all lysines *shaded* and the three lysines unique to Gα$_{i2}$ denoted by *asterisks*. *M1–M3*, the respective lysine to arginine mutations engineered into the YFP-tagged Gα$_{i2}$. CEM cells were transfected with CD8, WT, or the indicated Gα$_{i2}$ mutant and HA-tagged Nef or empty HA vector. Extracts of transfected cells were adjusted for equivalent CD8 expression and analyzed by immunoblotting using mAb against YFP for detecting Gα$_{i2}$. *Numbers* at the *bottom* are relative (%) pixel densities of Gα$_{i2}$ averaged from two experiments. *B*, M1 mutant is more efficient than the WT Gα$_{i2}$-YFP in rectifying Nef-induced G-protein signaling (by intracellular Ca^{2+} flux) defect. CEM cells were nucleofected with CD8, and YFP-tagged WT or M1 Gα$_{i2}$ CD8 transfectants were analyzed for CXCL12-driven intracellular Ca^{2+} flux as described in the legend to Fig. 3. *C*, YFP-tagged WT, but not the M1 Gα$_{i2}$, was internalized and co-localized with Nef-enriched vesicular structures. HeLa cells in coverglass chambers were co-transfected with YFP-tagged WT or M1 Gα$_{i2}$ mutant with Nef-CerFP or CerFP and processed for live microscopy. Cerulean is *green*, and YFP is *red*.

Given that Gq stability and functionality were unaltered by Nef, migration of certain leukocyte subtypes, such as DCs and monocytes, might be differentially regulated *in vivo*.

Nef is a short-lived protein produced early in the HIV life cycle; Nef protein and fragments are packaged within nascent HIV particles and may be delivered to newly infected cells (71). Non-infected cells may also be subject to Nef effects either by its secretion by infected cells or by its transfer via intercellular nanotubular conduits from infected to non-infected cells, which can alter cellular function (72, 73) and membrane dynamics causing a transfer of infected cell signaling to recipient cells (74). The targeting of Gα$_{i2}$ for destruction by Nef in infected as well as in nearby non-infected cells provides several potential advantages for HIV. First, disabling responsiveness to chemoattractants prevents cells from leaving a nidus of infection, thereby promoting cell-to-cell spread of the virus. Second, because of the importance of T cell migration for T cell function, disruption of directed T cell migration will impair the induction of effective immunity. Third, a sharp reduction in Gα$_{i2}$ will impair the sequestration of Gβγ subunits. Freed Gβγ subunits can activate downstream effectors that can provide signals that promote viral replication as well as effect cell survival. Fourth, decreased Gα$_{i2}$ removes its tonic inhibition of adenylyl cyclase isoforms, increasing cAMP levels and PKA activity, which can also enhance HIV replication (75–77). Fifth, because heterotrimeric G-proteins also function in GPCR-independent signaling pathways involved in intracellular trafficking and cell division (78–80), Nef-induced Gα$_{i2}$ loss may impact T cell function by affecting these pathways.

Although the Nef-induced chemotaxis defect may derive in part from its effects on other signaling events, such as PAK2-mediated cofilin deregulation (29) or inappropriate DOCK2/ELMO1-driven Rac activation uncoupled from chemokine receptor signaling (24), we have shown that Nef-induced loss of Gα$_{i2}$ probably trumps these because it impacts the earliest events in chemokine signaling. HIV, by expressing Nef, has chosen to target Gα$_{i2}$ for destruction. Nef probably does so by usurping a normal cellular mechanism that regulates Gα$_{i2}$ stability. Nef-induced loss of Gα$_{i2}$ in lymphocytes will profoundly affect their function and may impact signaling pathways that impact HIV replication.

Acknowledgments—We thank Philip Murphy (LMI, NIAID, National Institutes of Health) for critical review of the manuscript. We thank Steven Becker (Biological Imaging Section, RTB, NIAID, National Institutes of Health) for technical advice. We thank Adriano Marchese (Stritch School of Medicine, Loyola University, Chicago) for the generous supply of numerous reagents and technical advice and Bruce Conklin (University of California, San Francisco) for the Gq$_{i5}$ chimera.

REFERENCES

1. Rossi, D., and Zlotnik, A. (2000) The biology of chemokines and their receptors. *Annu. Rev. Immunol.* **18,** 217–242
2. Wurbel, M. A. (2000) The chemokine TECK is expressed by thymic and intestinal epithelial cells and attracts double- and single-positive thymocytes expressing the TECK receptor CCR9. *Eur. J. Immunol.* **30,** 262–271
3. Kwan, J., and Killeen, N. (2004) CCR7 directs the migration of thymocytes into the thymic medulla. *J. Immunol.* **172,** 3999–4007
4. Trampont, P. C., Tosello-Trampont, A.-C., Shen, Y., Duley, A. K., Sutherland, A. E., Bender, T. P., Littman, D. R., and Ravichandran, K. S. (2010) CXCR4 acts as a costimulator during thymic β-selection. *Nat. Immunol.* **11,** 162–170
5. Bromley, S. K., Thomas, S. Y., and Luster, A. D. (2005) Chemokine receptor CCR7 guides T cell exit from peripheral tissues and entry into afferent lymphatics. *Nat. Immunol.* **6,** 895–901
6. Debes, G. F., Arnold, C. N., Young, A. J., Krautwald, S., Lipp, M., Hay, J. B., and Butcher, E. C. (2005) Chemokine receptor CCR7 required for T lymphocyte exit from peripheral tissues. *Nat. Immunol.* **6,** 889–894
7. Charo, I. F., and Ransohoff, R. M. (2006) The many roles of chemokines and chemokine receptors in inflammation. *N. Engl. J. Med.* **354,** 610–621
8. Sallusto, F., Geginat, J., and Lanzavecchia, A. (2004) Central memory and effector memory T cell subsets. Function, generation, and maintenance. *Annu. Rev. Immunol.* **22,** 745–763
9. Brainard, D. M., Tager, A. M., Misdraji, J., Frahm, N., Lichterfeld, M., Draenert, R., Brander, C., Walker, B. D., and Luster, A. D. (2007) Decreased $CXCR3^+$ CD8 T cells in advanced human immunodeficiency virus infection suggest that a homing defect contributes to cytotoxic T-lymphocyte dysfunction. *J. Virol.* **81,** 8439–8450
10. Bromley, S. K., Mempel, T. R., and Luster, A. D. (2008) Orchestrating the orchestrators. Chemokines in control of T cell traffic. *Nat. Immunol.* **9,** 970–980
11. Delon, J., Stoll, S., and Germain, R. N. (2002) Imaging of T-cell interactions with antigen presenting cells in culture and in intact lymphoid tissue. *Immunol. Rev.* **189,** 51–63
12. Garside, P., Ingulli, E., Merica, R. R., Johnson, J. G., Noelle, R. J., and Jenkins, M. K. (1998) Visualization of specific B and T lymphocyte interactions in the lymph node. *Science* **281,** 96–99
13. Pantaleo, G., and Fauci, A. S. (1996) Immunopathogenesis of HIV infection. *Annu. Rev. Microbiol.* **50,** 825–854
14. Kinter, A., Arthos, J., Cicala, C., and Fauci, A. S. (2000) Chemokines, cytokines and HIV: a complex network of interactions that influence HIV pathogenesis. *Immunol. Rev.* **177,** 88–98
15. Kourtis, A. P., Ibegbu, C., Nahmias, A. J., Lee, F. K., Clark, W. S., Sawyer, M. K., and Nesheim, S. (1996) Early progression of disease in HIV-infected infants with thymus dysfunction. *N. Engl. J. Med.* **335,** 1431–1436
16. Chrobak, P., Simard, M. C., Bouchard, N., Ndolo, T. M., Guertin, J., Hanna, Z., Dave, V., and Jolicoeur, P. (2010) HIV-1 Nef disrupts maturation of $CD4^+$ T cells through CD4/Lck modulation. *J. Immunol.* **185,** 3948–3959
17. Hanna, Z., Kay, D. G., Rebai, N., Guimond, A., Jothy, S., and Jolicoeur, P. (1998) Nef harbors a major determinant of pathogenicity for an AIDS-like disease induced by HIV-1 in transgenic mice. *Cell* **95,** 163–175
18. Skowronski, J., Parks, D., and Mariani, R. (1993) Altered T cell activation and development in transgenic mice expressing the HIV-1 *nef* gene. *EMBO J.* **12,** 703–713
19. Hrecka, K., Swigut, T., Schindler, M., Kirchhoff, F., and Skowronski, J. (2005) Nef proteins from diverse groups of primate lentiviruses downmodulate CXCR4 to inhibit migration to the chemokine stromal derived factor 1. *J. Virol.* **79,** 10650–10659
20. Michel, N., Ganter, K., Venzke, S., Bitzegeio, J., Fackler, O. T., and Keppler, O. T. (2006) The Nef protein of human immunodeficiency virus is a broad-spectrum modulator of chemokine receptor cell surface levels that acts independently of classical motifs for receptor endocytosis and Galphai signaling. *Mol. Biol. Cell* **17,** 3578–3590
21. Roeth, J. F., and Collins, K. L. (2006) Human immunodeficiency virus type 1 Nef. Adapting to intracellular trafficking pathways. *Microbiol. Mol. Biol. Rev.* **70,** 548–563
22. Kirchhoff, F., Schindler, M., Specht, A., Arhel, N., and Münch, J. (2008) Role of Nef in primate lentiviral immunopathogenesis. *Cell Mol. Life Sci.* **65,** 2621–2636
23. Laguette, N., Brégnard, C., Benichou, S., and Basmaciogullari, S. (2010) Human immunodeficiency virus (HIV) type-1, HIV-2 and simian immunodeficiency virus Nef proteins. *Mol. Aspects Med.* **31,** 418–433
24. Janardhan, A., Swigut, T., Hill, B., Myers, M. P., and Skowronski, J. (2004) HIV-1 Nef binds the DOCK2-ELMO1 complex to activate Rac and inhibit lymphocyte chemotaxis. *PLoS Biol.* **2,** E6
25. Park, I. W., and He, J. J. (2009) HIV-1 Nef-mediated inhibition of T cell migration and its molecular determinants. *J. Leukoc. Biol.* **86,** 1171–1178
26. Campbell, E. M., Nunez, R., and Hope, T. J. (2004) Disruption of the actin cytoskeleton can complement the ability of Nef to enhance human immunodeficiency virus type 1 infectivity. *J. Virol.* **78,** 5745–5755
27. Haller, C., Rauch, S., Michel, N., Hannemann, S., Lehmann, M. J., Keppler, O. T., and Fackler, O. T. (2006) The HIV-1 pathogenicity factor Nef interferes with maturation of stimulatory T-lymphocyte contacts by modulation of N-Wasp activity. *J. Biol. Chem.* **281,** 19618–19630
28. Quaranta, M. G., Mattioli, B., Spadaro, F., Straface, E., Giordani, L., Ramoni, C., Malorni, W., and Viora, M. (2003) HIV-1 Nef triggers Vav-mediated signaling pathway leading to functional and morphological differentiation of dendritic cells. *FASEB J.* **17,** 2025–2036
29. Stolp, B., Reichman-Fried, M., Abraham, L., Pan, X., Giese, S. I., Hannemann, S., Goulimari, P., Raz, E., Grosse, R., and Fackler, O. T. (2009) HIV-1 Nef interferes with host cell motility by deregulation of Cofilin. *Cell Host Microbe* **6,** 174–186
30. Lu, T. C., He, J. C., Wang, Z. H., Feng, X., Fukumi-Tominaga, T., Chen, N., Xu, J., Iyengar, R., and Klotman, P. E. (2008) HIV-1 Nef disrupts the podocyte actin cytoskeleton by interacting with diaphanous interacting protein. *J. Biol. Chem.* **283,** 8173–8182
31. Yi, L., Rosales, T., Rose, J. J., Chaudhury, B., Knutson, J. R., and Venkatesan, S. (2010) HIV-1 Nef binds a subpopulation of MHC-I throughout its trafficking itinerary and down-regulates MHC-I by perturbing both anterograde and retrograde trafficking. *J. Biol. Chem.* **285,** 30884–30905
32. Rose, J. J., Foley, J. F., Murphy, P. M., and Venkatesan, S. (2004) On the mechanism and significance of ligand-induced internalization of human neutrophil chemokine receptors CXCR1 and CXCR2. *J. Biol. Chem.* **279,** 24372–24386
33. Venkatesan, S., Petrovic, A., Locati, M., Kim, Y. O., Weissman, D., and Murphy, P. M. (2001) A membrane-proximal basic domain and cysteine cluster in the C-terminal tail of CCR5 constitute a bipartite motif critical for cell surface expression. *J. Biol. Chem.* **276,** 40133–40145
34. Arrode, G., Hegde, R., Jin, Y., Singh, D. K., Narayan, O., and Cheboune, Y. (2008) Nef modulates the immunogenicity of Gag encoded in a non-infectious HIV DNA vaccine. *Vaccine* **26,** 3795–3804
35. Gibson, S. K., and Gilman, A. G. (2006) Gialpha and Gbeta subunits both define selectivity of G protein activation by α2-adrenergic receptors. *Proc. Natl. Acad. Sci. U.S.A.* **103,** 212–217
36. Conklin, B. R., Farfel, Z., Lustig, K. D., Julius, D., and Bourne, H. R. (1993) Substitution of three amino acids switches receptor specificity of Gqα to that of Giα. *Nature* **363,** 274–276
37. Krumins, A. M., and Gilman, A. G. (2006) Targeted knockdown of G protein subunits selectively prevents receptor-mediated modulation of effectors and reveals complex changes in non-targeted signaling proteins. *J. Biol. Chem.* **281,** 10250–10262
38. Rose, J. J., Foley, J. F., Yi, L., Herren, G., and Venkatesan, S. (2008) Cholesterol is obligatory for polarization and chemotaxis but not for endocytosis and associated signaling from chemoattractant receptors in human neutrophils. *J. Biomed. Sci.* **15,** 441–461
39. Choe, E. Y., Schoenberger, E. S., Groopman, J. E., and Park, I. W. (2002) HIV Nef inhibits T cell migration. *J. Biol. Chem.* **277,** 46079–46084
40. Lee, C. M., Gala, S., Stewart, G. J., and Williamson, P. (2008) The proline-rich region of HIV-1 Nef affects CXCR4-mediated chemotaxis in Jurkat T cells. *Viral Immunol.* **21,** 347–354
41. Macia, E., Ehrlich, M., Massol, R., Boucrot, E., Brunner, C., and Kirchhausen, T. (2006) Dynasore, a cell-permeable inhibitor of dynamin. *Dev. Cell* **10,** 839–850
42. Marchese, A., and Benovic, J. L. (2001) Agonist-promoted ubiquitination

of the G protein-coupled receptor CXCR4 mediates lysosomal sorting. *J. Biol. Chem.* **276,** 45509–45512
43. Marchese, A., Raiborg, C., Santini, F., Keen, J. H., Stenmark, H., and Benovic, J. L. (2003) The E3 ubiquitin ligase AIP4 mediates ubiquitination and sorting of the G protein-coupled receptor CXCR4. *Dev. Cell* **5,** 709–722
44. Bhandari, D., Robia, S. L., and Marchese, A. (2009) The E3 ubiquitin ligase atrophin interacting protein 4 binds directly to the chemokine receptor CXCR4 via a novel WW domain-mediated interaction. *Mol. Biol. Cell* **20,** 1324–1339
45. Ingham, R. J., Raaijmakers, J., Lim, C. S., Mbamalu, G., Gish, G., Chen, F., Matskova, L., Ernberg, I., Winberg, G., and Pawson, T. (2005) The Epstein-Barr virus protein, latent membrane protein 2A, co-opts tyrosine kinases used by the T cell receptor. *J. Biol. Chem.* **280,** 34133–34142
46. Otte, L., Wiedemann, U., Schlegel, B., Pires, J. R., Beyermann, M., Schmieder, P., Krause, G., Volkmer-Engert, R., Schneider-Mergener, J., and Oschkinat, H. (2003) WW domain sequence activity relationships identified using ligand recognition propensities of 42 WW domains. *Protein Sci.* **12,** 491–500
47. Winberg, G., Matskova, L., Chen, F., Plant, P., Rotin, D., Gish, G., Ingham, R., Ernberg, I., and Pawson, T. (2000) Latent membrane protein 2A of Epstein-Barr virus binds WW domain E3 protein-ubiquitin ligases that ubiquitinate B-cell tyrosine kinases. *Mol. Cell Biol.* **20,** 8526–8535
48. Harvey, K. F., and Kumar, S. (1999) Nedd4-like proteins. An emerging family of ubiquitin-protein ligases implicated in diverse cellular functions. *Trends Cell Biol.* **9,** 166–169
49. Hu, H., Columbus, J., Zhang, Y., Wu, D., Lian, L., Yang, S., Goodwin, J., Luczak, C., Carter, M., Chen, L., James, M., Davis, R., Sudol, M., Rodwell, J., and Herrero, J. J. (2004) A map of WW domain family interactions. *Proteomics* **4,** 643–655
50. Pirozzi, G., McConnell, S. J., Uveges, A. J., Carter, J. M., Sparks, A. B., Kay, B. K., and Fowlkes, D. M. (1997) Identification of novel human WW domain-containing proteins by cloning of ligand targets. *J. Biol. Chem.* **272,** 14611–14616
51. Lu, P. J., Zhou, X. Z., Shen, M., and Lu, K. P. (1999) Function of WW domains as phosphoserine- or phosphothreonine-binding modules. *Science* **283,** 1325–1328
52. Lee, C. H., Leung, B., Lemmon, M. A., Zheng, J., Cowburn, D., Kuriyan, J., and Saksela, K. (1995) A single amino acid in the SH3 domain of Hck determines its high affinity and specificity in binding to HIV-1 Nef protein. *EMBO J.* **14,** 5006–5015
53. Lee, C. H., Saksela, K., Mirza, U. A., Chait, B. T., and Kuriyan, J. (1996) Crystal structure of the conserved core of HIV-1 Nef complexed with a Src family SH3 domain. *Cell* **85,** 931–942
54. Kirchhoff, F., Münch, J., Carl, S., Stolte, N., Mätz-Rensing, K., Fuchs, D., Haaft, P. T., Heeney, J. L., Swigut, T., Skowronski, J., and Stahl-Hennig, C. (1999) The human immunodeficiency virus type 1 *nef* gene can to a large extent replace simian immunodeficiency virus *nef in vivo*. *J. Virol.* **73,** 8371–8383
55. Marotti, L. A., Jr., Newitt, R., Wang, Y., Aebersold, R., and Dohlman, H. G. (2002) Direct identification of a G protein ubiquitination site by mass spectrometry. *Biochemistry* **41,** 5067–5074
56. Wang, Y., Marotti, L. A., Jr., Lee, M. J., and Dohlman, H. G. (2005) Differential regulation of G protein α subunit trafficking by mono- and polyubiquitination. *J. Biol. Chem.* **280,** 284–291
57. Torres, M. P., Lee, M. J., Ding, F., Purbeck, C., Kuhlman, B., Dokholyan, N. V., and Dohlman, H. G. (2009) G protein mono-ubiquitination by the Rsp5 ubiquitin ligase. *J. Biol. Chem.* **284,** 8940–8950
58. Busconi, L., Guan, J., and Denker, B. M. (2000) Degradation of heterotrimeric $G\alpha_o$ subunits via the proteosome pathway is induced by the hsp90-specific compound geldanamycin. *J. Biol. Chem.* **275,** 1565–1569
59. Fischer, T., De Vries, L., Meerloo, T., and Farquhar, M. G. (2003) Promotion of $G\alpha_{i3}$ subunit down-regulation by GIPN, a putative E3 ubiquitin ligase that interacts with RGS-GAIP. *Proc. Natl. Acad. Sci. U.S.A.* **100,** 8270–8275
60. Ogasawara, J., Sakurai, T., Rahman, N., Kizaki, T., Hitomi, Y., Ohno, H., and Izawa, T. (2004) Acute exercise alters $G\alpha_{i2}$ protein expressions through the ubiquitin-proteasome proteolysis pathway in rat adipocytes. *Biochem. Biophys. Res. Commun.* **323,** 1109–1115
61. Naviglio, S., Pagano, M., Romano, M., Sorrentino, A., Fusco, A., Illiano, F., Chiosi, E., Spina, A., and Illiano, G. (2004) Adenylate cyclase regulation via proteasome-mediated modulation of $G\alpha_s$ levels. *Cell. Signal.* **16,** 1229–1237
62. Tang, T., Gao, M. H., Miyanohara, A., and Hammond, H. K. (2008) $G\alpha_q$ reduces cAMP production by decreasing $G\alpha_s$ protein abundance. *Biochem. Biophys. Res. Commun.* **377,** 679–684
63. Hamilton, M. H., Cook, L. A., McRackan, T. R., Schey, K. L., and Hildebrandt, J. D. (2003) γ2 subunit of G protein heterotrimer is an N-end rule ubiquitylation substrate. *Proc. Natl. Acad. Sci. U.S.A.* **100,** 5081–5086
64. Obin, M., Lee, B. Y., Meinke, G., Bohm, A., Lee, R. H., Gaudet, R., Hopp, J. A., Arshavsky, V. Y., Willardson, B. M., and Taylor, A. (2002) Ubiquitylation of the transducin $\beta\gamma$ subunit complex. Regulation by phosducin. *J. Biol. Chem.* **277,** 44566–44575
65. Cappell, S. D., Baker, R., Skowyra, D., and Dohlman, H. G. (2010) Systematic analysis of essential genes reveals important regulators of G protein signaling. *Mol. Cell* **38,** 746–757
66. Yang, L. V., Radu, C. G., Wang, L., Riedinger, M., and Witte, O. N. (2005) G_i-independent macrophage chemotaxis to lysophosphatidylcholine via the immunoregulatory GPCR G2A. *Blood* **105,** 1127–1134
67. Sozzani, S., Zhou, D., Locati, M., Rieppi, M., Proost, P., Magazin, M., Vita, N., van Damme, J., and Mantovani, A. (1994) Receptors and transduction pathways for monocyte chemotactic protein-2 and monocyte chemotactic protein-3. Similarities and differences with MCP-1. *J. Immunol.* **152,** 3615–3622
68. Maghazachi, A. A., al-Aoukaty, A., and Schall, T. J. (1994) C-C chemokines induce the chemotaxis of NK and IL-2-activated NK cells. Role for G proteins. *J. Immunol.* **153,** 4969–4977
69. Shi, G., Partida-Sánchez, S., Misra, R. S., Tighe, M., Borchers, M. T., Lee, J. J., Simon, M. I., and Lund, F. E. (2007) Identification of an alternative $G\alpha_q$-dependent chemokine receptor signal transduction pathway in dendritic cells and granulocytes. *J. Exp. Med.* **204,** 2705–2718
70. Misra, R. S., Shi, G., Moreno-Garcia, M. E., Thankappan, A., Tighe, M., Mousseau, B., Kusser, K., Becker-Herman, S., Hudkins, K. L., Dunn, R., Kehry, M. R., Migone, T. S., Marshak-Rothstein, A., Simon, M., Randall, T. D., Alpers, C. E., Liggitt, D., Rawlings, D. J., and Lund, F. E. (2010) $G\alpha_q$-containing G proteins regulate B cell selection and survival and are required to prevent B cell-dependent autoimmunity. *J. Exp. Med.* **207,** 1775–1789
71. Welker, R., Kottler, H., Kalbitzer, H. R., and Kräusslich, H. G. (1996) Human immunodeficiency virus type 1 Nef protein is incorporated into virus particles and specifically cleaved by the viral proteinase. *Virology* **219,** 228–236
72. Qiao, X., He, B., Chiu, A., Knowles, D. M., Chadburn, A., and Cerutti, A. (2006) Human immunodeficiency virus 1 Nef suppresses CD40-dependent immunoglobulin class switching in bystander B cells. *Nat. Immunol.* **7,** 302–310
73. Xu, W., Santini, P. A., Sullivan, J. S., He, B., Shan, M., Ball, S. C., Dyer, W. B., Ketas, T. J., Chadburn, A., Cohen-Gould, L., Knowles, D. M., Chiu, A., Sanders, R. W., Chen, K., and Cerutti, A. (2009) HIV-1 evades virus-specific IgG2 and IgA responses by targeting systemic and intestinal B cells via long-range intercellular conduits. *Nat. Immunol.* **10,** 1008–1017
74. Muratori, C., Cavallin, L. E., Krätzel, K., Tinari, A., De Milito, A., Fais, S., D'Aloja, P., Federico, M., Vullo, V., Fomina, A., Mesri, E. A., Superti, F., and Baur, A. S. (2009) Massive secretion by T cells is caused by HIV Nef in infected cells and by Nef transfer to bystander cells. *Cell Host Microbe* **6,** 218–230
75. Amella, C. A., Sherry, B., Shepp, D. H., and Schmidtmayerova, H. (2005) Macrophage inflammatory protein 1α inhibits postentry steps of human immunodeficiency virus type 1 infection via suppression of intracellular cyclic AMP. *J. Virol.* **79,** 5625–5631
76. Cartier, C., Hemonnot, B., Gay, B., Bardy, M., Sanchiz, C., Devaux, C., and Briant, L. (2003) Active cAMP-dependent protein kinase incorporated within highly purified HIV-1 particles is required for viral infectivity and interacts with viral capsid protein. *J. Biol. Chem.* **278,** 35211–35219
77. Rabbi, M. F., Al-Harthi, L., and Roebuck, K. A. (1997) TNFα cooperates

with the protein kinase A pathway to synergistically increase HIV-1 LTR transcription via downstream TRE-like cAMP response elements. *Virology* **237,** 422–429

78. Cho, H., and Kehrl, J. H. (2007) Localization of Giα proteins in the centrosomes and at the midbody. Implication for their role in cell division. *J. Cell Biol.* **178,** 245–255
79. Slessareva, J. E., Routt, S. M., Temple, B., Bankaitis, V. A., and Dohlman, H. G. (2006) Activation of the phosphatidylinositol 3-kinase Vps34 by a G protein α subunit at the endosome. *Cell* **126,** 191–203
80. Wilkie, T. M., and Kinch, L. (2005) New roles for Gα and RGS proteins. Communication continues despite pulling sisters apart. *Curr. Biol.* **15,** R843–R854